# Supplementary Material

## Asteroid clusters similar to asteroid pairs

---

### Convergence of cluster members in secular angles

Analysis of ages of asteroid families, namely time elapsed since their formation, attracted considerable attention over the past decade or so (see Nesvorný et al., 2015, for a review and further references). Researchers made attempts to determine the age of every known family, but this task was found too ambitious. Most importantly, the available methods become very uncertain in the case of old families (ages larger than a billion of years or so). On the other side of the spectrum, namely in the case of young families (ages less than 10 Myr or so), prospects to constrain the age were found more optimistic. This is because in this category one can use the most straightforward way to approach the problem, namely direct backward integration of orbits of the family members from today's epoch back to the supposed origin of the family. The ideal indicator of the family origin would be a configuration of the fragments very close to each other with a small relative velocities; this is the outcome of the parent body fragmentation. In the imperfect world, where our ability to reconstruct the past fragment configuration using orbital integration is limited, we need less ambitious, but practical, criterion for the origin of the family. This has been set by Nesvorný et al. (2002, 2003), who studied the first two examples of very young families (a $\simeq 5.8$ Myr old Karin family and a $\simeq 8.3$ Myr old Veritas family). In particular, these authors limited themselves to monitor convergence of the secular angles – longitude of node $\Omega$ and longitude of perihelion $\varpi$ – of the family members to the largest fragment. Note that in families older than $1-3$ Myr, these angles are randomly distributed between $0^\circ$ and $360^\circ$ at the present epoch. At origin, though, their dispersion must have been less then a degree, in smaller families even a fraction of a degree. The goal of the method in Nesvorný et al. (2002, 2003) thus was to follow the backward integration of the family members until the nodal and pericenter dispersions, $\Delta\Omega$ and $\Delta\varpi$, were small and became to increase again. In the category of Myr-old families with tens to hundreds of known fragments, such as Karin and Veritas, the achievable best performance was $\Delta\Omega \simeq \Delta\varpi \simeq 30^\circ - 40^\circ$. This does not look too impressive, compared to the sub-degree goal. However, it was quickly recognized that an important missing element in the original model was the Yarkovsky effect. While primarily affecting orbital semimajor axis $a$, this phenomenon has an important indirect effect of the secular angles, because their precession frequency very sensitively depends on $a$. With this improvement, Nesvorný and Bottke (2004) were able to reach convergence dispersion level $\Delta\Omega \simeq \Delta\varpi \simeq 10^\circ$ for the Karin family (see also Carruba

et al. 2016), and Carruba et al. (2017) had $\Delta\Omega \simeq \Delta\varpi \simeq 15^\circ$ for the Veritas family. Similar results were also obtained for $\simeq 3.6$ Myr old Iannini/Nele family (Carruba et al. 2017, in preparation), or $1.5 - 1.9$ Myr old Gibbs and Lorre families (Novaković et al. 2012, 2014). Little worse performance, $\Delta\Omega \simeq 30^\circ$, was observed in the case of $\simeq 6.9$ Myr old Theobalda family (Novaković et al. 2010). The reason for this slightly worse result was orbital chaoticity induced by the weak mean motion resonances crossing the zone of this family. Apart from this effect, the non-ideal performance in attempts to achieve convergence of the secular angles is due to stochastic perturbations from massive bodies in the main belt (mainly Ceres, Vesta, Pallas and Juno) and often badly constrained orbits for small members in the families.

Better results were expected from the analysis of sub-Myr old families. This is because in their case, even the present-day $\Omega$ and $\varpi$ values of their members are clustered within typically few to tens of degrees (e.g., Nesvorný et al. 2006; Nesvorný and Vokrouhlický 2006). Additionally, these families have usually a small number of members. Therefore at convergence, degree to sub-degree dispersions $\Delta\Omega$ and $\Delta\varpi$ were achievable. In order to link them more directly with the initial event of fragment dispersion from the parent body, Nesvorný and Vokrouhlický (2006) proposed to combine $\Delta\Omega$ and $\Delta\varpi$ into a single target function

$$\Delta V = na\sqrt{(\sin I\Delta\Omega)^2 + 0.5\,(e\Delta\varpi)^2}\,, \tag{1}$$

where $na \simeq 18 - 20$ km/s is the mean orbital velocity of the family members, $e$ and $I$ their mean eccentricity and inclination values. Modulo the problem of unknown true/mean anomaly of the parent body at the moment of family formation, $\Delta V$ is a direct measure of the characteristic dispersal velocity of the fragments. Therefore, it is best compared with the estimated escape velocity $v_{\rm esc}$ from the parent body. Nesvorný and Vokrouhlický (2006) were hoping for solutions $\Delta V \leq v_{\rm esc}$, and assumed only those be valid (additionally, they required a certain interval of differences in mean anomalies $|\Delta M| < 180^\circ$, typically tens of degrees, of the converging fragments). This was indeed achievable for the best examples of very young and compact families containing only three to four members. Given the lesson from Myr-old and larger families, it is however, not surprising that in some cases we need to slightly relax the convergence limit on $\Delta V$ and allow up to $C\,v_{\rm esc}$ limit, where $C \simeq (1 - 20)$. Note that for $v_{\rm esc}$ of few m/s, this still represents dispersal levels $\Delta\Omega$ and $\Delta\varpi$ of the order of a degree or less, thus fairly good. The particular value of $C$ for a given family/cluster depends on a number of factors such as number of members, chaoticity of their orbits due to underlying web of mean motion resonances, vulnerability to close encounters with Ceres, Vesta and other massive asteroids in the main belt, accuracy with which the initial data of the orbits are known, age of the family (such that for older families we quickly loose accuracy in their reconstruction due to previously mentioned effects), etc. As a result, the precise value of $C$ is partly a matter of experimenting. In the best performing cases we will have $C = 1$, and additionally constrain mean anomaly values of the converging fragments to some range $\Delta M$ about the largest body in the family (see Nesvorný and Vokrouhlický 2006). For less optimum cases, we will

have $C > 1$, and no constraint on the mean anomalies.

As described above, backward integration of orbits of members in young asteroid families allows to constrain its age. While this game may be less or more accurate, e.g. by necessity to choose larger $C$ factors than unity, in the same time the method allows to discriminate between true family members (whose orbits converge) and interlopers from the background main belt population of asteroids (whose orbits do not converge). It is actually this aspect of the method that interests us more in the context of our work. Note, that we primarily need to estimate the cumulative mass of the secondaries versus the primary in the studied clusters (Sec. 3), while obtaining the cluster's age is merely a by-product of this work.

Our numerical runs were carried out using the `swift` integrator package with the Yarkovsky effect included. We typically used $200 - 300$ clones for each of the asteroids. These represent different starting initial conditions (aka geometric clones, all chosen according to the current orbit determination) and also different values of the Yarkovsky effect (randomly set in between estimated minimum and maximum values). We output the results every four years, and we group the converging cases (i.e., when $\Delta V \leq C\, v_{\rm esc}$) in 10 or 20 kyr bins. Integrations are usually stopped at the 2 Myr epoch, but extended to $4-5$ Myr when needed. Even with a rather low number of clones of each of the asteroids, the complete number of identifications between all of them would be huge (billions and often much more). The CPU requirements for such a complete search would be too large, so we pre-selected tens to hundreds of thousands of clone identifications of our integrated orbits and only these were checked at every output time, which was 4 years (except for the cluster of (66583), where the output time was 200 days). The bin width of the histograms in Suppl. Figs. 1–10 is 20 kyr, except for the clusters of (22280) and (39991) in Suppl. Figs. 8 and 9 where it is 10 kyr.

Simulations were done for all the clusters discussed in the main text of the paper. Here, however, we report only new results. This is because in some cases, the same methodology has already been published in the literature, namely for the clusters: (1270) Datura, (16598) Brugmansia and (21509) Lucascavin in Nesvorný and Vokrouhlický (2006) (see also Vokrouhlický et al. 2009), (2384) Schulhof in Vokrouhlický et al. (2016), and (18777) Hobson in Rosaev and Plávalová (2017). First, we present raw results from our integrations, followed by their summary.

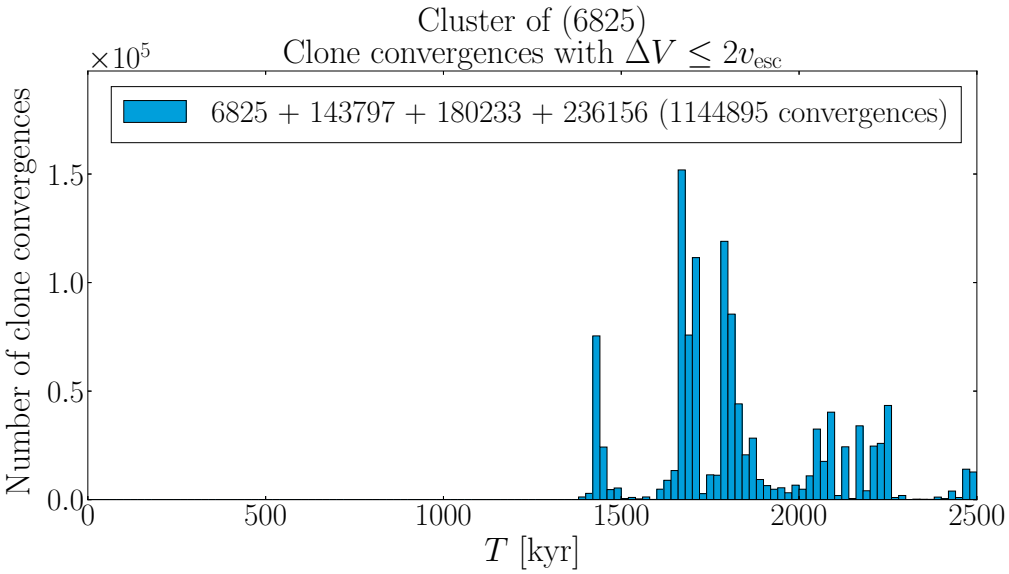


Suppl. Fig. 1. Distribution of times of orbital clone convergences for the four members of the cluster of (6825) Irvine. For each asteroid, we generated 200 clones and we performed 300 thousand selections of orbits from the generated set.

*(6825) Irvine* – This is a unique cluster living in an isolation at the bottomost part of the main belt, already in a region where density of asteroids is very low. Therefore it is very easily recognizable even without sophisticated identification methods. Pravec and Vokrouhlický (2009) reported its age between 1.4 and 1.8 Myr. Supplementary Figure 1 confirms that most of the converging solutions are indeed in this range. We used a slightly relaxed criterion with $C = 2$. This is because this family is strongly influenced by the nearby $\nu_6$ resonance. The critical angle $\sigma = \varpi - \varpi_6$ ($\varpi_6$ is Saturn's longitude of perihelion) slowly circulates with a period of $\simeq$ 440 kyr (as expected from the proper frequency $g \simeq 31.2$ arcsec/yr). This seems to have repercussions in the convergence statistics seen in Fig. 1. These effects, together with age larger than a Myr and small members in this cluster, make the convergence efforts somewhat troubling, hence the $C > 1$ value.

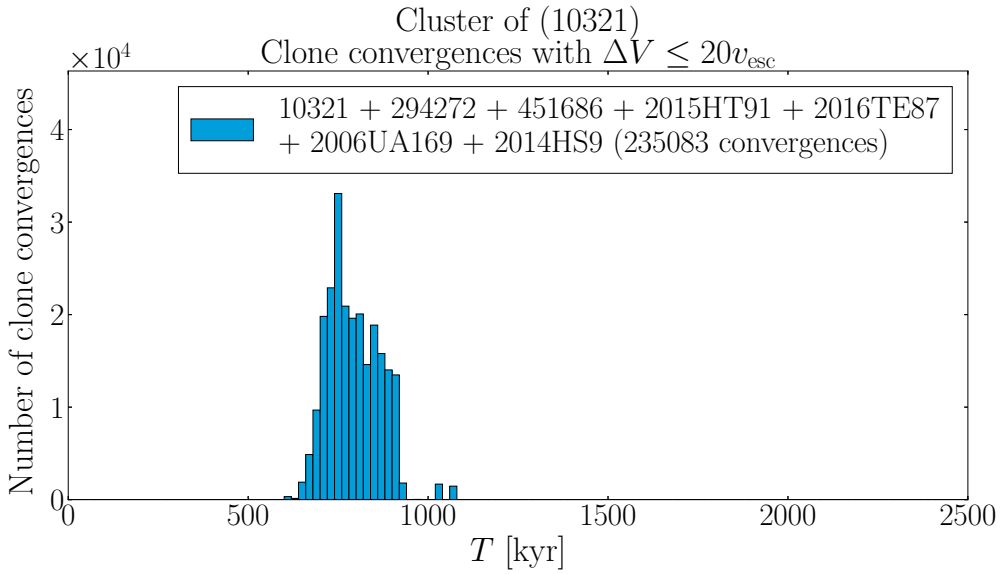


Suppl. Fig. 2. Distribution of times of orbital clone convergences for the six members of the cluster of (10321) Rampo. For each asteroid, we generated 250 clones and we performed 260 thousand selections of orbits from the generated set.

*(10321) Rampo* – This cluster resides in the inner main belt quite near to the J10/3 mean motion resonance. However, at low eccentricity this resonance is still narrow-enough not to significantly affect dynamics in this cluster. The reason why we need to choose $C = 20$, see Suppl. Fig. 2, is mainly due to other effects: (i) large number of members in this cluster, and (ii) rather poorly constrained orbits of the small members. With a limited number of clones we are using, many of them may result in simply fake past evolution. Yet, the possibility of convergence of all members within less than a degree is a convincing argument for an age between 600 and 900 kyr (Suppl. Fig. 2), as already guessed by Pravec and Vokrouhlický (2009). Note that the nominal orbits at present epoch have the secular angles spread in an interval of nearly 15°.

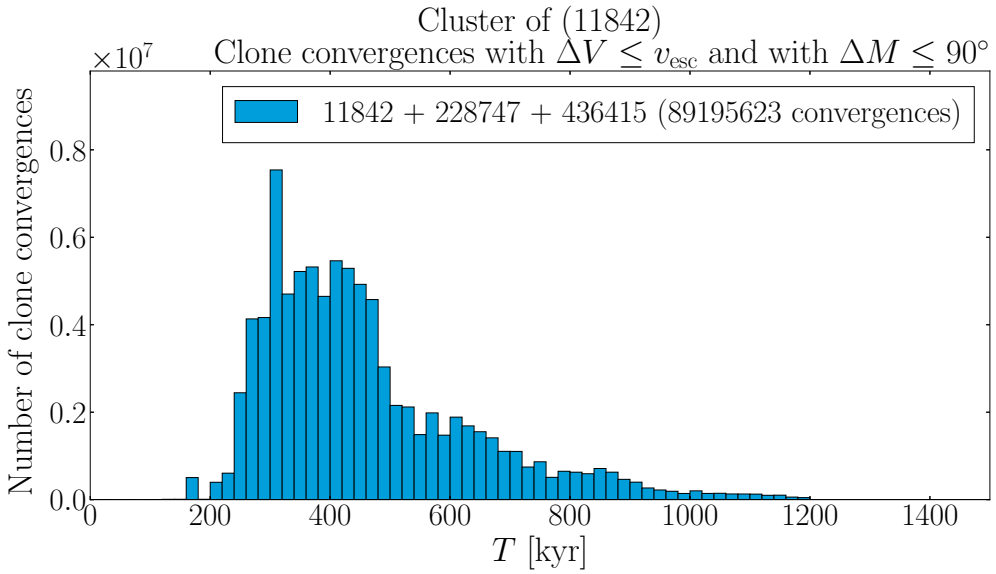


Suppl. Fig. 3. Distribution of times of orbital clone convergences for the three members of the cluster of (11842) Kap'bos. For each asteroid, we generated 300 clones and we performed 650 thousand selections of orbits from the generated set.

*(11842) Kap'bos* – Supplementary Figure 3 shows a number of converging solutions for this cluster with $C = 1$ and even restricting to the mean anomaly range of 90° around the largest fragment. The high number of successful convergence cases indicates a very robust solution in this case. There are two favorable circumstances for such a good result. First, the cluster presently contains only three members. Second, this is a very tight cluster such that their current orbits are very close to each other (less than half a degree apart in the secular angles and less than 0.001 au in osculating semimajor axis).

*(14627) Emilkowalski* – The Emilkowalski family presents an interesting puzzle (see discussion in Section 2.6). Nesvorný and Vokrouhlický (2006) found a reasonable convergence of the largest four members within $220 \pm 30$ kyr, though admittedly the orbit of (126761) 2002 DW10 was noticed to be affected by a yet-to-be-identified resonant phenomenon (see Fig. 2 of Nesvorný and Vokrouhlický 2006). For that reason, its convergence in perihelion was not perfect (see bottom and right panel on Fig. 2 of Nesvorný and Vokrouhlický 2006).

The group of the three small and more distant secondaries discovered in this work has a very good convergence to (14627) Emilkowalski between 1.0 and 1.5 Myr ago (see Suppl. Fig. 4). We used a fairly reasonable value $C = 2$ which indicates a very robust convergence. Note that it corresponds to dispersion $\Delta\Omega \simeq \Delta\varpi \simeq 0.15°$, while the present orbits of all these members have angular distances from (14627) Emilkowalski between 5° and 10°.

Additionally we also performed the following two test runs: (i) we considered a sub-cluster of best-converging Emilkowalski members with young age (Suppl. Fig. 5), and (ii) we added asteroid (126761) 2002 DW10 to the older group of Emilkowalski members (Suppl. Fig. 6). This is because we have seen that convergence of (126761) 2002 DW10 among the younger group is somewhat problematic. However, we found that even among the older group, this orbits causes slight degradation of the results and we needed to increase $C$ value to 5. It is possible that the orbit of (126761) 2002 DW10 underwent a close encounter to some of massive bodies in the main belt or feels perturbing effects from some fine-tuned resonant phenomenon. In any case, the possibility of two fragmentation events in the Emilkowalski cluster is an interesting topic for the future study.

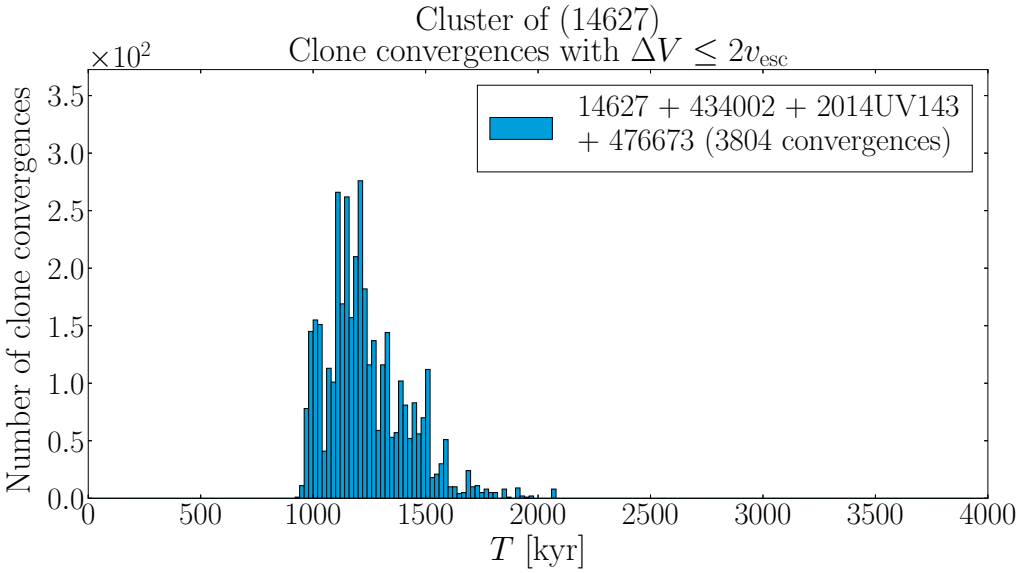


Suppl. Fig. 4. Distribution of times of orbital clone convergences for the three distant, smaller and recently discovered secondaries of the cluster of (14627) Emilkowalski. For each asteroid, we generated 300 clones and we performed 250 thousand selections of orbits from the generated set.

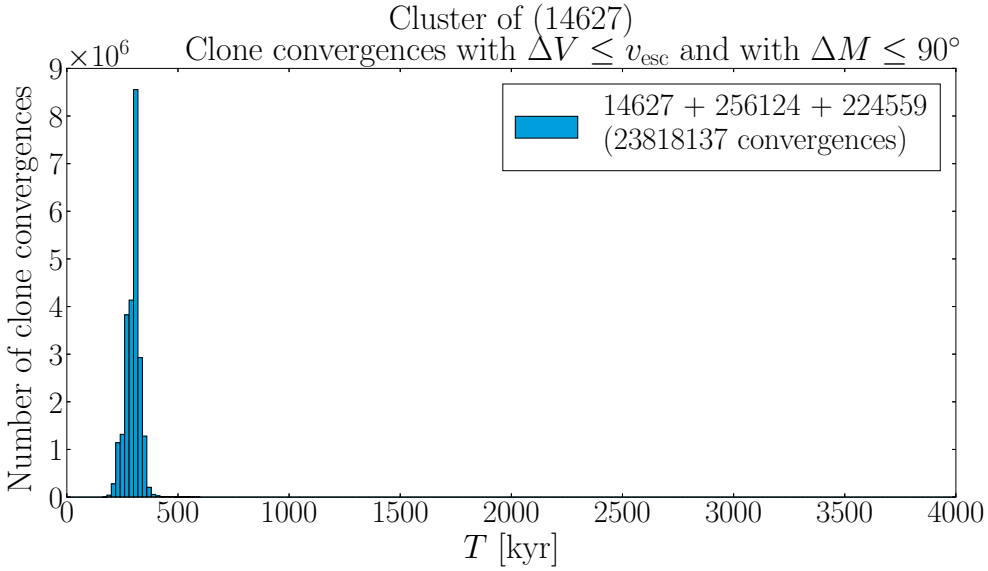


Suppl. Fig. 5. Distribution of times of orbital clone convergences for the three tight members of the cluster of (14627) Emilkowalski. For each asteroid, we generated 300 clones and we performed 500 thousand selections of orbits from the generated set.

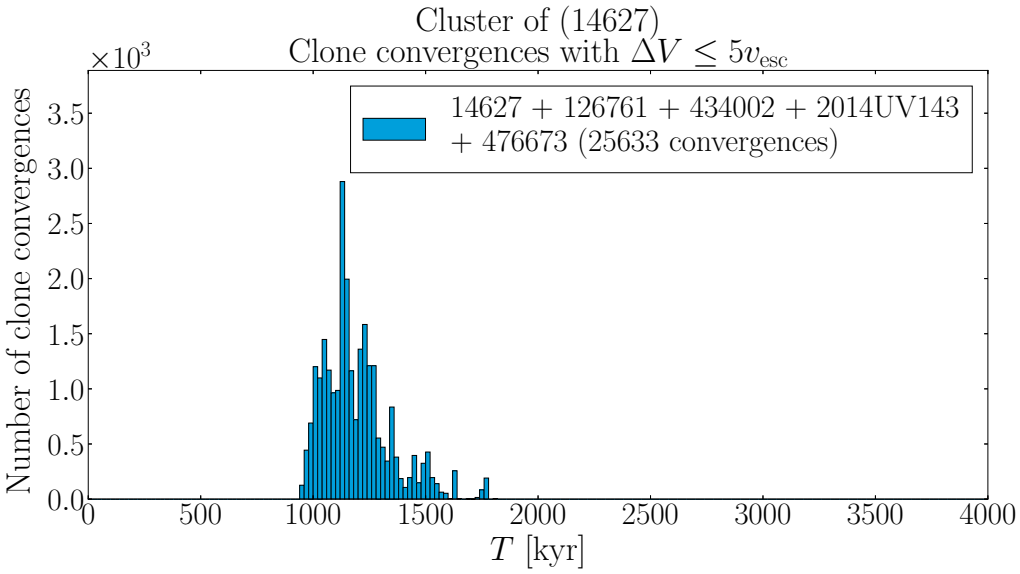


Suppl. Fig. 6. Distribution of times of orbital clone convergences for the largest secondary (126761) 2002 DW10 and the three distant, smaller and recently discovered secondaries of the cluster of (14627) Emilkowalski. For each asteroid, we generated 300 clones and we performed 160 thousand selections of orbits from the generated set.

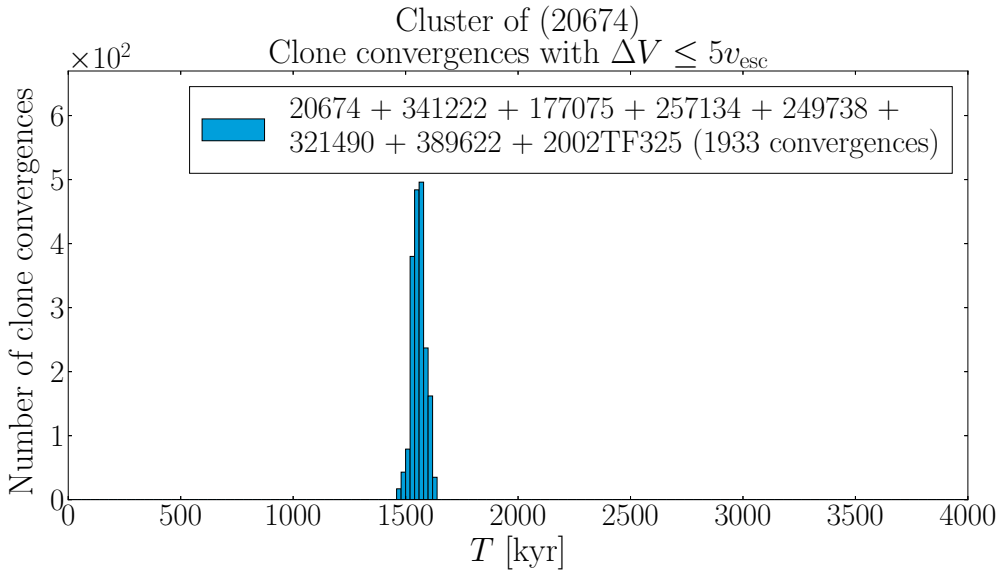


Suppl. Fig. 7. Distribution of times of orbital clone convergences for the eight members of the cluster of (20674) 1999 VT1(called the Gibbs cluster in Novaković et al. 2014). For each asteroid, we generated 300 clones and we performed 244 thousand selections of orbits from the generated set.

*(20674) 1999 VT1 (Gibbs)* – Given the relatively large number of members of this cluster we used $C = 5$ value. Nevertheless, results shown in Suppl. Fig. 7 indicate a very good convergence for 8 members of the cluster, equivalent to a sub-degree dispersions $\Delta\Omega$ and $\Delta\varpi$. This is largely better than shown in Novaković et al. (2014), perhaps because these authors also included (140429) 2001 TQ96 in their analysis (see discussion in Section 2.9). Nevertheless, they showed a possibility of a simultaneous convergence below 10° dispersions of the secular angles. This is considerably tighter than individual scatter of the present-day secular angles within more than 30° range. Additionally, our age solution agrees well with that in Novaković et al. (2014).

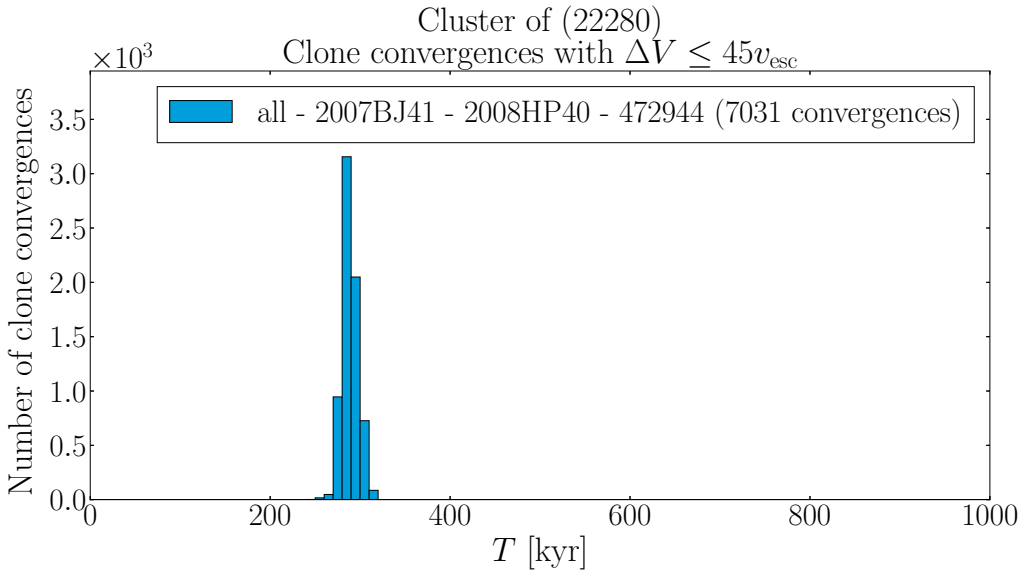


Suppl. Fig. 8. Distribution of times of orbital clone convergences for the 16 members of the cluster of (22280) Mandragora. For each asteroid, we generated 300 clones and we performed 330 thousand selections of orbits from the generated set.

*(22280) Mandragora* – This cluster contains the highest number of members among the clusters studied in this paper. In our analysis of clone convergences, we used all of them except two members with poorly determined orbits and the secondary (472944) 2015 GH28 that is on a chaotic orbit. The large number of orbits, and strong influence by the J9/4 mean motion resonance in some cases, made us to use $C = 45$, exceptionally large in our context. Note, however, that it corresponds to dispersions in the secular angles less than 10° (in fact, $\Delta\Omega \simeq 3°$ and $\Delta\varpi \simeq 5°$). Given the standards used in young families such as Karin, mentioned above, this is still a very good result. Note that the current orbits, especially those very near to J9/4 resonance, have their longitude of pericenter many tens of degrees away from that of (22280) Mandragora. With this perspective, we consider the convergence in this also acceptable.

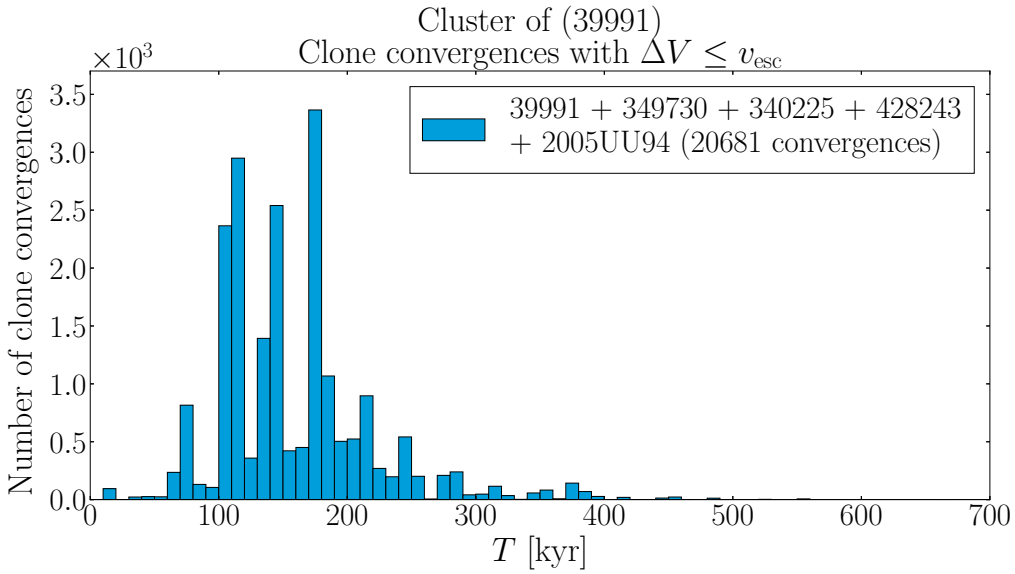


Suppl. Fig. 9. Distribution of times of orbital clone convergences for the five members of the cluster of (39991) Iochroma. For each asteroid, we generated 300 clones and we performed 26 thousand selections of orbits from the generated set.

*(39991) Iochroma* – This cluster offers a very good convergence solution as seen in Suppl. Fig. 9, where we used $C = 1$ limit. The favorable circumstance is a very tight clustering of the orbits at present, with secular angles within two degrees from each other. The odds that may slightly trouble the convergence attempts are two: (i) the orbits in this cluster are affected by a weak mean motion resonance 5J+3S-2, and (ii) all four members, apart from (39991) Iochroma, are very small asteroids, which implies a possibly strong influence by the Yarkovsky effect. The limited number of clones used could mean that many would correspond to fake past evolution. Luckily, the age within the past 500 kyr helps to alleviate this problem.

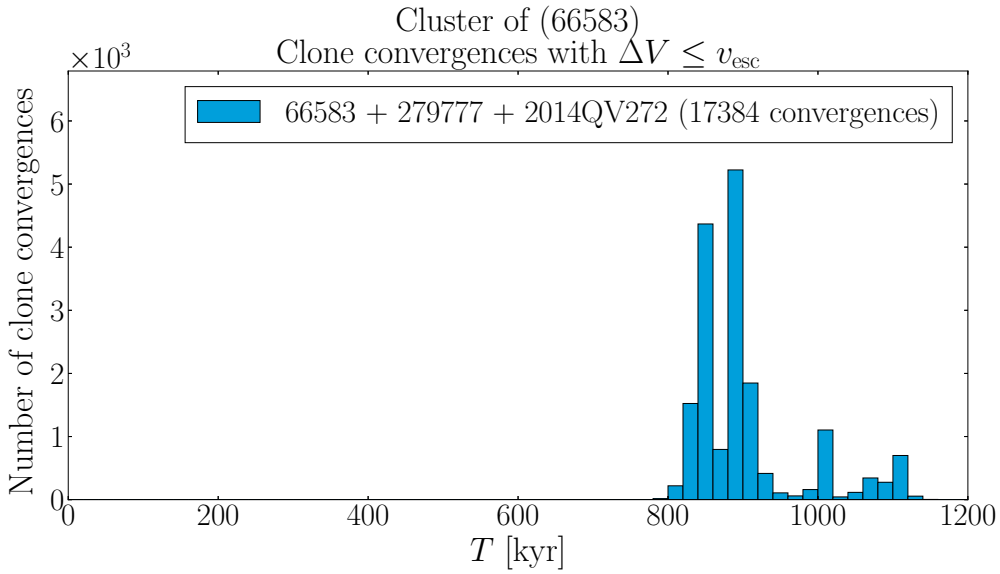


Suppl. Fig. 10. Distribution of times of orbital clone convergences for the three multi-opposition members of the cluster of (66583) Nicandra. For each asteroid, we generated 400 clones and we performed 98 thousand selections of orbits from the generated set.

*(66583) Nicandra* – In this case we considered only three multi-opposition members and disregarded two single-opposition cases (Table 1 in the main text), whose orbits are very uncertain. With this restriction, the convergence is very good, we used $C = 1$ and restricted mean anomaly to $|\Delta M| < 90^\circ$ for the converging cases (Suppl. Fig. 10). This corresponds to only a fraction of a degree dispersions $\Delta\Omega$ and $\Delta\varpi$, in spite of the current differences of about ten degrees in the osculating orbits.

Suppl. Table 1
Summary of the clone convergence results

| | Cluster | Age estimate (kyr) | Remark |
|---|---|---|---|
| (6825) | Irvine | $1790^{+460}_{-350}$ | $C = 2$, $\nu_6$ resonance |
| (10321) | Rampo | $780^{+130}_{-\ 90}$ | $C = 20$, numerous small members |
| (11842) | Kap'bos | $420^{+410}_{-160}$ | $C = 1$, $\lvert\Delta M\rvert < 90°$ |
| (14627) | Emilkowalski | $300^{+\ 40}_{-\ 70}$ | $C = 1$, $\lvert\Delta M\rvert < 90°$, young group |
| (14627) | Emilkowalski | $1200^{+370}_{-210}$ | $C = 2$, distant members only (old group) |
| (14627) | Emilkowalski | $1160^{+350}_{-160}$ | $C = 5$, distant members with (126761) (old group) |
| (20674) | 1999 VT1 | $1560^{+\ 50}_{-\ 50}$ | $C = 5$, without (140429) |
| (22280) | Mandragora | $290^{+\ 20}_{-\ 20}$ | $C = 45$, without three members |
| (39991) | Iochroma | $140^{+130}_{-\ 70}$ | $C = 1$ |
| (66583) | Nicandra | $890^{+210}_{-\ 60}$ | $C = 1$ |

*Summary* – We used the previously described results to summarize age estimations for the clusters discussed in this paper. The methodology uses convergence of the secular angles as discussed above. We constructed cumulative distribution of the converging solutions in time and computed its (i) median $T_{\rm M}$, and (ii) 5% and 95% percentils $T_5$ and $T_{95}$. These data are used to characterize the family age in a form: $T_{\rm M}{}^{+(T_{95}-T_{\rm M})}_{-(T_{\rm M}-T_5)}$. The results are summarized in Suppl. Table 1.

**Photometric observations of asteroid cluster members**

We carried out photometric observations using our standard asteroid lightcurve photometry techniques. The data were corrected for light-travel time and standard calibration with bias, dark and flatfield frames was applied to all images. We analysed the observations using our methods described in Pravec et al. (2006).

The individual observing sessions in the Supplementary Information are identified with the date given to the nearest 10th of a day to the midtime of the session's observational interval. All dates and times in Suppl. Fig. 11 to 39 are asterocentric JD (UTC), i.e., they were light-time corrected. In Suppl. Table 2, there are listed the participating observatories, instruments and observers. We give references and descriptions of observational procedures on the individual observatories in following. The original digital data are available at `http://www.asu.cas.cz/~ppravec/astclusters_201702_lc_data.zip`

*Abastumani* – The observations at the Abastumani Astrophysical Observatory were carried out with the 0.7-m meniscus Maksutov telescope with FLI IMG6303E CCD camera in the primary focus (f/3). Observational method and reduction procedures at Abastumani were the same as we used at Simeiz (see below). The observations were made without filter.

*Kharkiv* – CCD photometry was done with the 0.7-m reflector at Chuguev Observatory of Kharkiv National University using the CCD camera IMG 47-10 ($1056 \times 1027$ pixels, $13 \times 13$ $\mu$m pixel) installed in Newtonian focus (f/4) equipped with a 3-lens focal corrector (0.951 arcsec/pixel, FOV $16.7 \times 16.3$ arcmin$^2$). The method of observations and data reduction were described in Krugly et al. (2002).

*La Silla* – For observations with the Danish 1.54-m telescope, we used the same or analogous procedures as those we used for observations from Ondřejov (see below) and for observations of Apophis (Pravec et al., 2014).

*Maidanak* – Observations were carried out at Maidanak Astronomical Observatory (Uzbekistan) with 1.5-m telescope AZT-22 (Cassegrain f/7.7), equipped with back-illuminated Fairchild 486 CCD camera ($4096 \times 4096$ CCD, $15 \times 15$ $\mu$m pixel, 0.27 arcsec/pixel, FOV $18.4 \times 18.4$ arcmin$^2$). The observations were carried out unfiltered to get higher S/N and they were reduced in the standard way with master-bias subtracting and median flat-field dividing. The aperture photometry of the asteroid and comparison stars in the images was done with the ASTPHOT package developed at DLR (Mottola et al. 1995). The effective radius of aperture was equal to $1-1.5\times$ the seeing that included more than 90% of the flux of a star or the asteroid. The relative photometry of the asteroid was done with typical errors in a range of 0.02–0.03 mag using an ensemble of comparision stars.

*Modra* – Observational system, data analysis and reduction process are described in Galád et al. (2007) and later they made use of tools provided by

Astrometry.net (Lang et al. 2010).

*Nauchny* – Procedures of observations and image reduction with the 2.6-m telescope of the Crimean Astrophysical Observatory were largely the same as we used at Kharkiv (see above). The CCD camera FLI PL4240 was used in the primary focus of the telescope (f/3.85). We observed without filter. During night the telescope was shifted several times between exposures in different directions. The night images were used for constructing a median flatfield (sky flat). The image reduction includes dark removal and correction using the sky flat.

*Ondřejov* – Observational system, data analysis and reduction process are described in Pravec et al. (2006).

*Rozhen* – At the Rozhen National Astronomical Observatory (Bulgaria), the observations were carried out with the 2-m Ritchey-Chretien reflector using CCD camera VersArray1300B ($1340 \times 1300$ pixels, $20 \times 20$ $\mu$m pixel) installed with a focal reducer FoReRo2 in the Cassegrain focus. The field of view was about 15 arcmin. The method of asteroid observations and reduction is described in Krugly et al. (2002). The observations were done through the standard R filter and reduced by means of subtracting a master-bias and normalizing on a median master-flat. The ASTPHOT package developed at DLR (Mottola et al. 1995) was used for aperture photometry of asteroid. Absolute photometry was done using observed standard stars with colors close to the solar ones taken from Skiff (2007). An accuracy of calibrated photometry is typically around 0.03 mag.

*Simeiz* – The observations were carried with a 1-m Ritchey-Chrétien telescope at Simeiz Department of the Crimean Astrophysical Observatory using camera FLI PL09000. The observations were made in the Johnson-Cousins photometric system. Standard procedure of image reduction included dark removal and flatfield correction. The aperture photometry was done with the AstPhot package described in Mottola et al. (1995). The differential lightcurves were calculated with respect to an ensemble of comparison stars by the method described in Erikson et al. (2000) and Krugly (2004).

*Skalnaté Pleso* – The photometric observations at the Skalnaté Pleso Observatory were carried with the 0.61-m f/4.3 reflector through the Cousins R filter and SBIG ST-10XME with $3 \times 3$ binning with resolution of 1.6 arcsec/px. CCD frames were reduced in standard way using bias, dark and flat field frames with IRAF tools. The images were photometrically reduced using the procedure described in Husárik and Kušnirák (2008).

*SRO* – The Sonoita Research Observatory (SRO) observations were collected with a 0.5-m folded Newtonian operating at f/4 and an SBIG STL-6303E with an image scale of 0.92 arcsec/pixel. The system was mounted on a Software Bisque Paramount ME. Image acquisition and observatory control are automated via DC-3 Dreams ACP. Integration times were 300 sec and images were unfiltered. The images were dark subtracted and flat fielded, then reduced using MIRA. The differential photometry was performed against an ensemble

of comparison stars for (11842) Kap'bos and against single comparison stars for (16598) Brugmansia. The images were examined for interfering stars and those images were discarded.

*Sugarloaf Mountain* – Observations at Sugarloaf Mountain Observatory were made using a 0.5-m, f/4.0 reflector on a Paramount ME mount. The imaging CCD was a SBIG ST-10XME cooled to −15°C, where images were taken through a clear filter. The image scale was 1.38 arcsec/pixel, and the fov was $25.0 \times 16.8$ arcmin$^2$. Derived magnitudes were estimated using a method inherent in the analysis software, *MPO Canopus*. The method is based on referencing a hybrid star catalog consisting mostly of 2MASS stars in the V band. Images were calibrated using master bias, dark and flat field images.

Suppl. Table 2
Observatories, Instruments and Observers/Reducers

| **Observatory** | **Telescope** | **Diameter (m)** | **Observers/Reducers** |
|---|---|---|---|
| Abastumani | | 0.7 | Inasaridze, Krugly, Kvaratskhelia, Ayvazian, Zhuzhunadze |
| Kharkiv | | 0.7 | Krugly |
| La Silla | Danish | 1.54 | Pravec, Kušnirák, Hornoch, Galád, Fatka |
| Maidanak | | 1.5 | Krugly, Burkhonov, Ehgamberdiev |
| Modra | | 0.60 | Galád, Világi, Gajdoš, Kornoš |
| Nauchny | | 2.6 | Rumyantsev, Krugly |
| Ondřejov | | 0.65 | Kušnirák, Hornoch, Vraštil |
| Rozhen | | 2.0 | Donchev, Borisov, Bonev, Krugly |
| Simeiz | | 1.0 | Gaftonyuk, Krugly |
| Skalnaté Pleso | | 0.61 | Husárik, Pikler, Červák |
| SRO | | 0.5 | Cooney, Gross, Terrell |
| Sugarloaf Mountain | | 0.50 | Pray |

**(6825) Irvine**

We observed this asteroid from Sugarloaf Mountain, Skalnaté Pleso, Modra, Ondřejov and Abastumani on 7 nights during 2011-12-28 to 2012-03-19. The Ondřejov run of 2012-03-18.8 was absolutely calibrated in the Cousins R system using Landolt (1992) standards to an accuracy level of 0.015 mag; the observations from the other stations were on relative (differential) magnitude scales. We derived a period of $3.61589 \pm 0.00005$ h. The lightcurve amplitude evolved, apparently in correlation with solar phase: it was 0.58 mag at solar phase 5° to 0.85 mag at solar phase 24° . The asteroid's mean absolute R magnitude is $H_R = 13.58 \pm 0.14$, assuming the slope parameter $G = 0.24 \pm 0.11$. These our results compare well to those obtained by Waszczak et al. (2015) in 2012: They observed a period of $P = 3.6156 \pm 0.0012$ h with an amplitude of 0.70 mag. Our lightcurve data are shown in Suppl. Fig. 11.

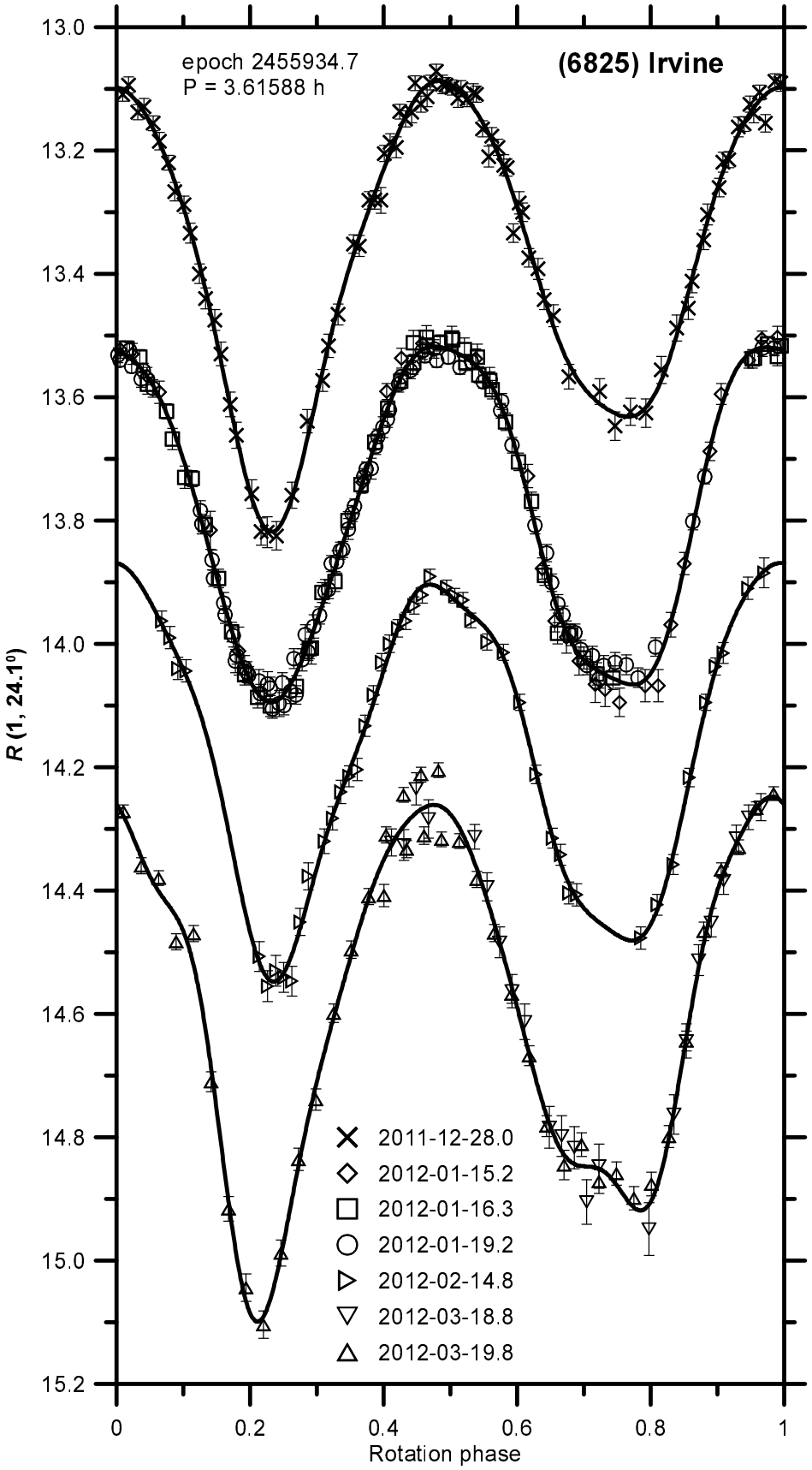


Suppl. Fig. 11. Rotational lightcurves of (6825) Irvine. The absolute R magnitude scale refers to the calibrated 2012-03-18.8 data (the bottom curve); the other data are on relative magnitude scales and their composite lightcurves were shifted in magnitude for clarity.

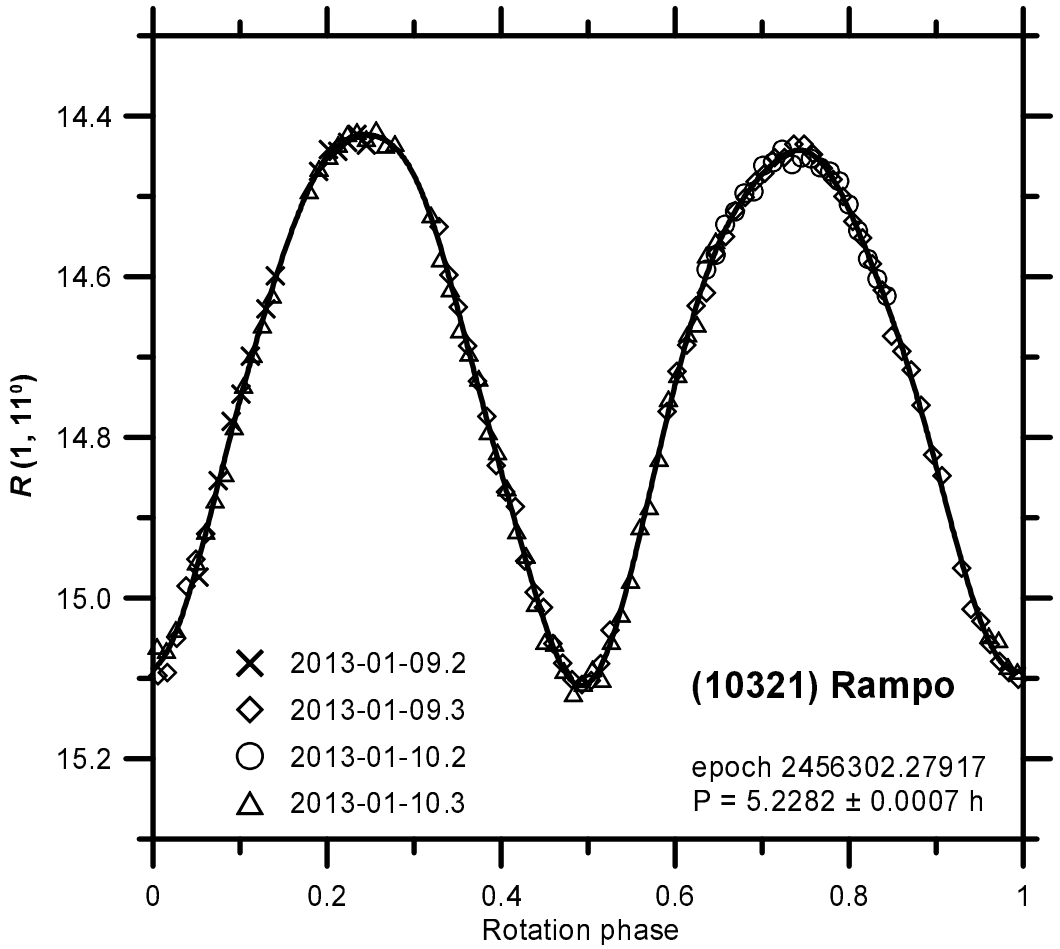


Suppl. Fig. 12. Rotational lightcurve of (10321) Rampo in 2013.

### (10321) Rampo

We observed this asteroid from La Silla on 2 nights 2013-01-09 and 10 and from Ondřejov on 1 night 2015-11-06. The observations were absolutely calibrated in the Johnson-Cousins VR system using Landolt (1992) standards to an accuracy level of 0.01–0.02 mag. From the 2013 observations, we derived a period of 5.2282 ± 0.0007 h. The lightcurve amplitude was 0.69 mag on 2013-01-09 to 10 and 0.51 mag on 2015-11-06. On 2013-01-09.3 we measured the color index $(V - R) = 0.500 \pm 0.01$. The mean absolute R magnitude was $H_R = 14.11 \pm 0.09$ and $14.08 \pm 0.09$ in 2013 and 2015, respectively, both derived assuming $G = 0.24 \pm 0.11$. Our lightcurve data are shown in Suppl. Figs. 12 and 13.

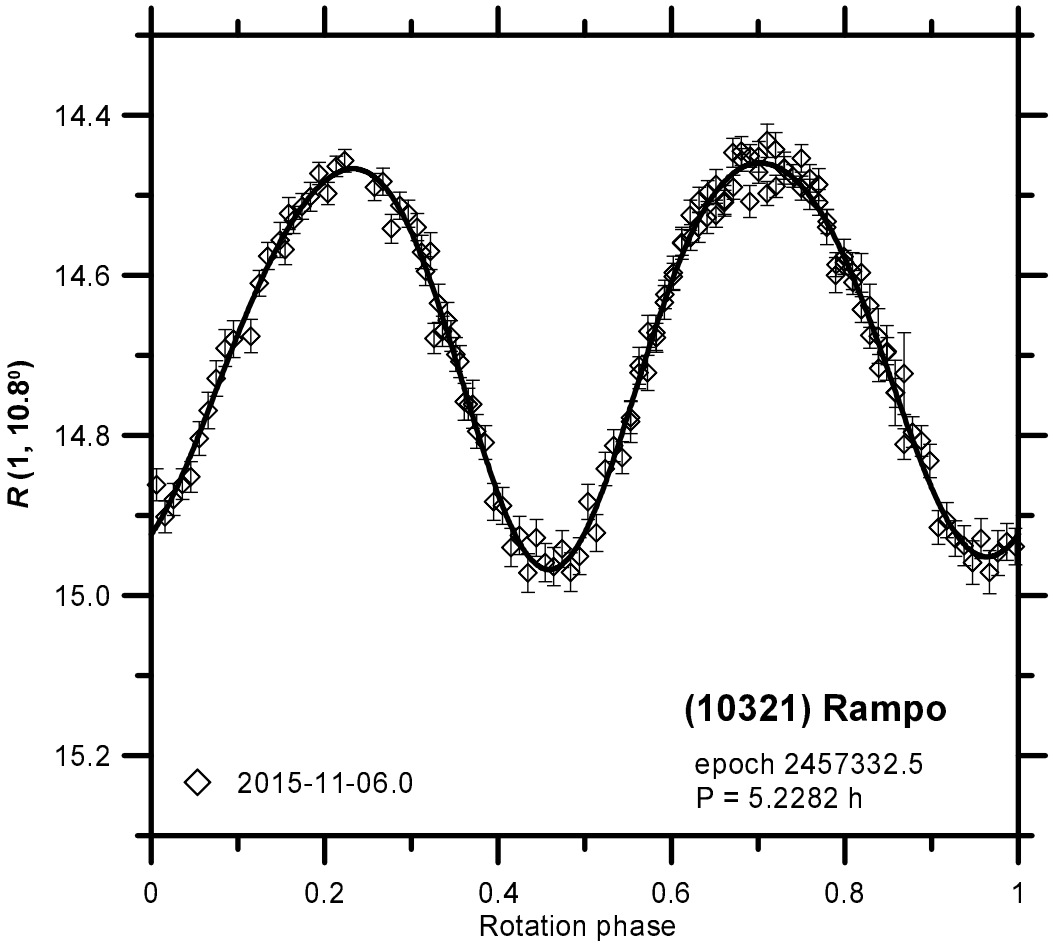


Suppl. Fig. 13. Rotational lightcurve of (10321) Rampo in 2015.

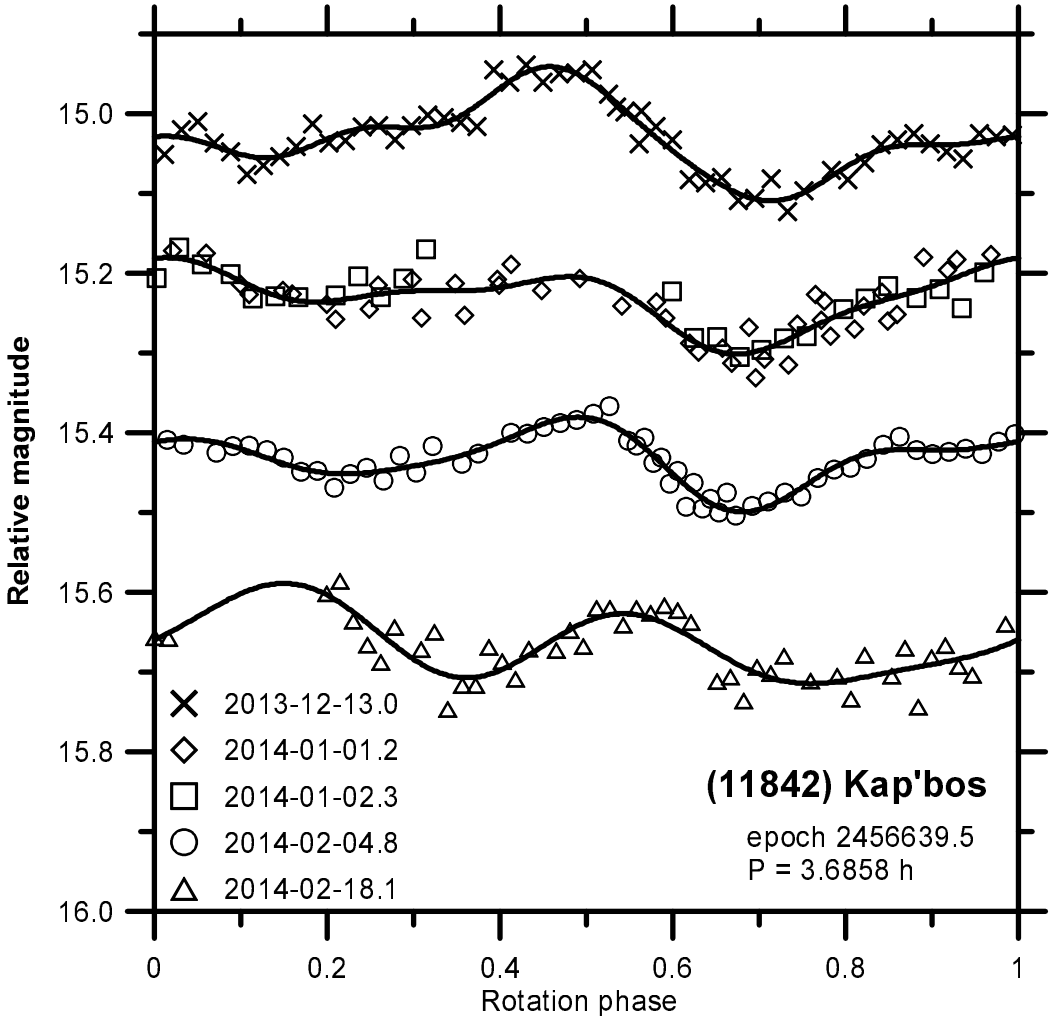


Suppl. Fig. 14. Rotational lightcurve of (11842) Kap'bos in 2013.

### (11842) Kap'bos

We observed this asteroid from Simeiz, Sugarloaf Mountain and SRO on 5 nights during 2013-12-13 to 2014-02-18 and from La Silla and Ondřejov on 4 nights during 2016-09-28 to 11-06. The La Silla run of 2016-11-06 was absolutely calibrated in the Johnson-Cousins VR system using Landolt (1992) standards to an accuracy level of 0.01 mag; the observations from the other stations were on relative (differential) magnitude scales. They are consistent with the period $3.68578 \pm 0.00009$ h by Pravec et al. (2010). The lightcurve amplitude evolved, apparently in correlation with solar phase: it was 0.10 mag at solar phase 6° to 0.17 mag at solar phase 21°. Our lightcurve data are shown in Suppl. Figs. 14 to 15.

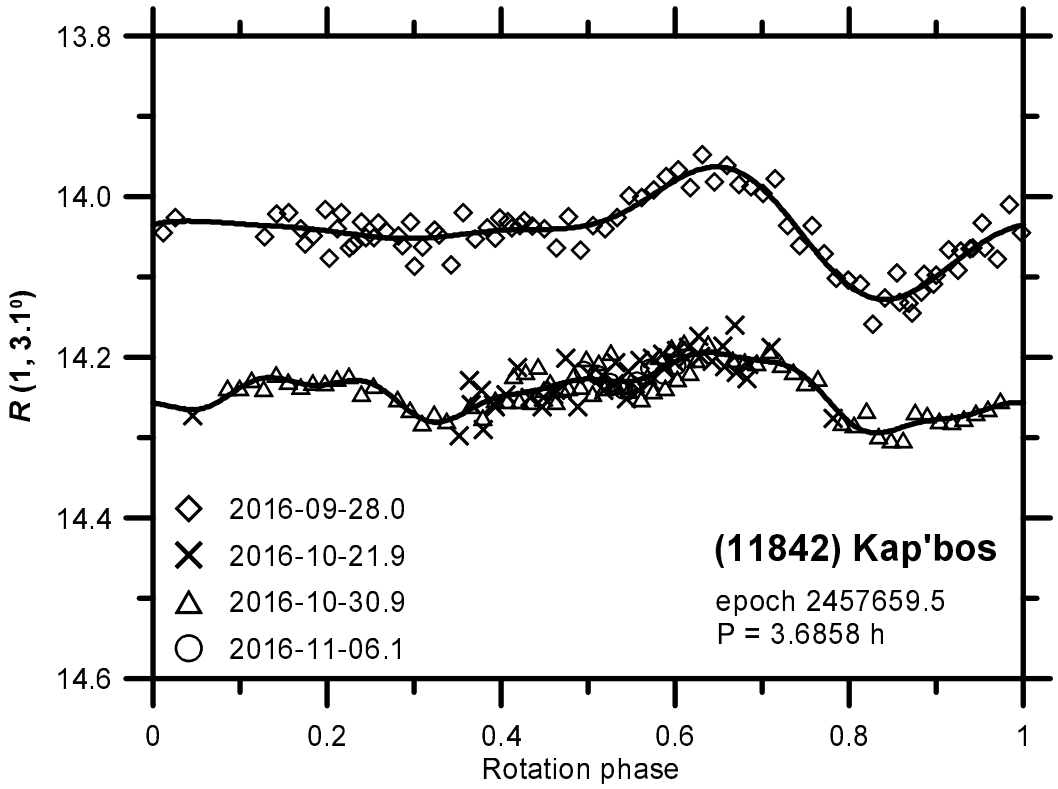


Suppl. Fig. 15. Rotational lightcurve of (11842) Kap'bos in 2016. The absolute R magnitude scale refers to the calibrated 2016-11-06.1 data (the bottom curve); the other data are on relative magnitude scales and they were shifted in magnitude for clarity.

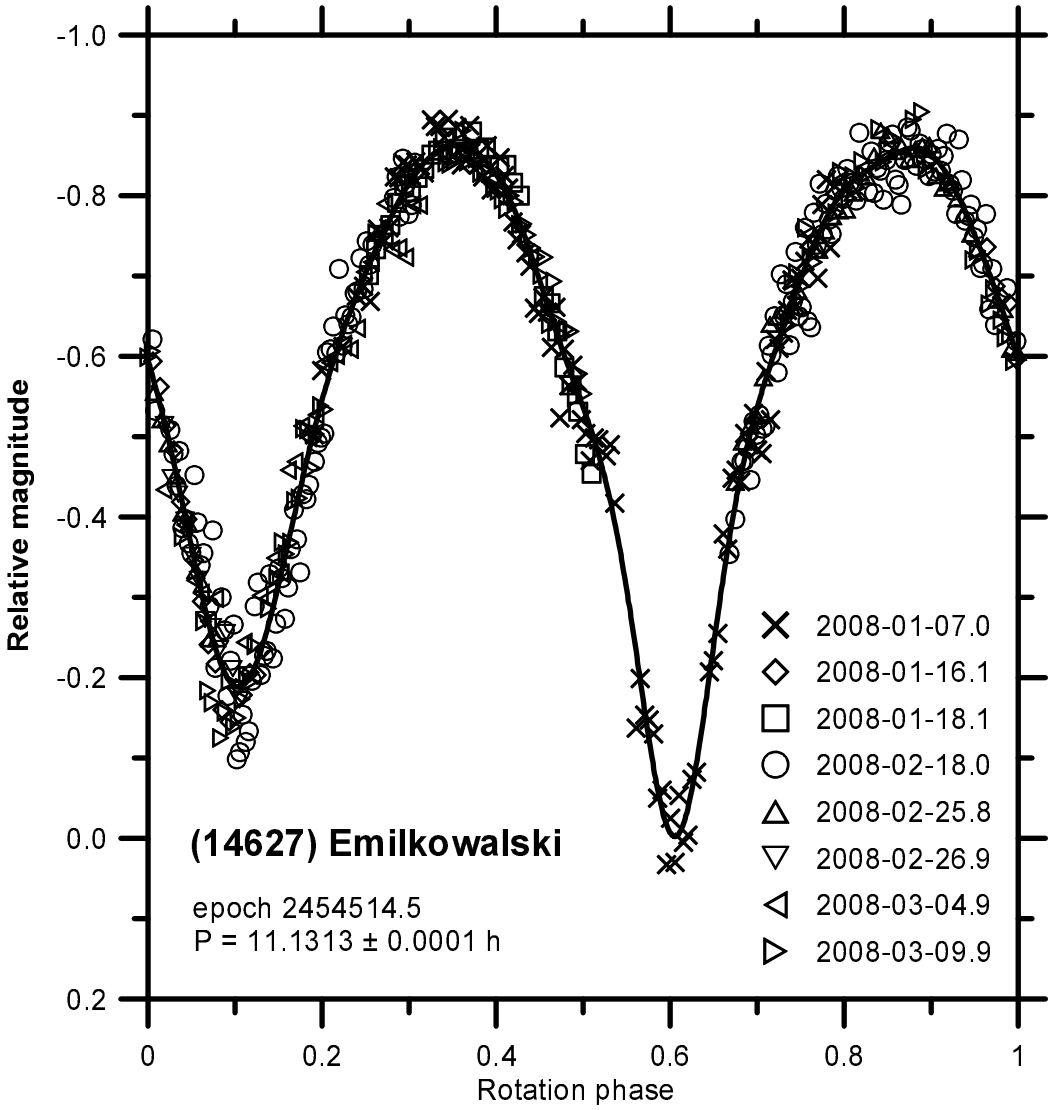


Suppl. Fig. 16. Rotational lightcurve of (14627) Emilkowalski in 2008.

**(14627) Emilkowalski**

We observed this asteroid from Simeiz and Kharkiv on 8 nights during 2008-01-07 to 03-09, from Ondřejov, Modra, Sugarloaf Mountain, Skalnaté Pleso and Abastumani on 13 nights during 2012-01-18 to 03-21, and from Abastumani on 6 nights during 2015-12-16 to 2016-02-09. The Ondřejov observations were absolutely calibrated in the Cousins R system using Landolt (1992) standards to an accuracy level of 0.015–0.02 mag; the observations from the other stations were on relative (differential) magnitude scales. We derived a period of $11.1313 \pm 0.0001$ h (synodic-sidereal uncertainty $\pm 0.0009$ h) and $11.131 \pm 0.002$ h from the 2008 and 2012 observations, respectively. The lightcurve amplitude changed, it was between 0.32 mag during 2015-12-16 to 2016-01-02 and 0.86 mag on 2008-01-07. We derived the asteroid's mean absolute R magnitude $H_R = 13.15 \pm 0.05$ and the slope parameter $G = -0.05 \pm 0.03$. Our lightcurve data are shown in Suppl. Figs. 16 to 18.

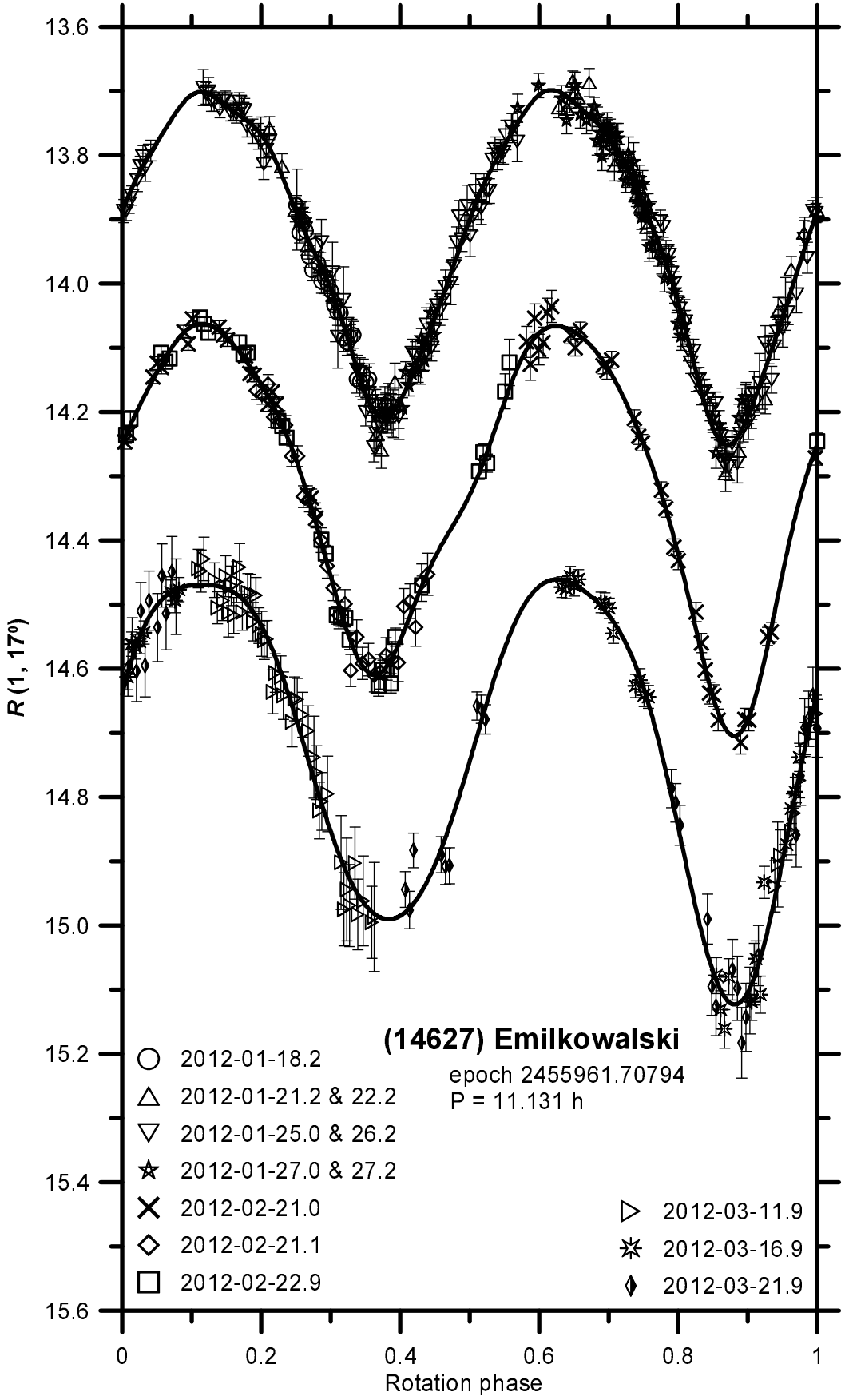


Suppl. Fig. 17. Rotational lightcurves of (14627) Emilkowalski in 2012. The magnitude scale refers to the middle composite lightcurve, the other two were shifted by −0.4 and +0.4 mag, for clarity.

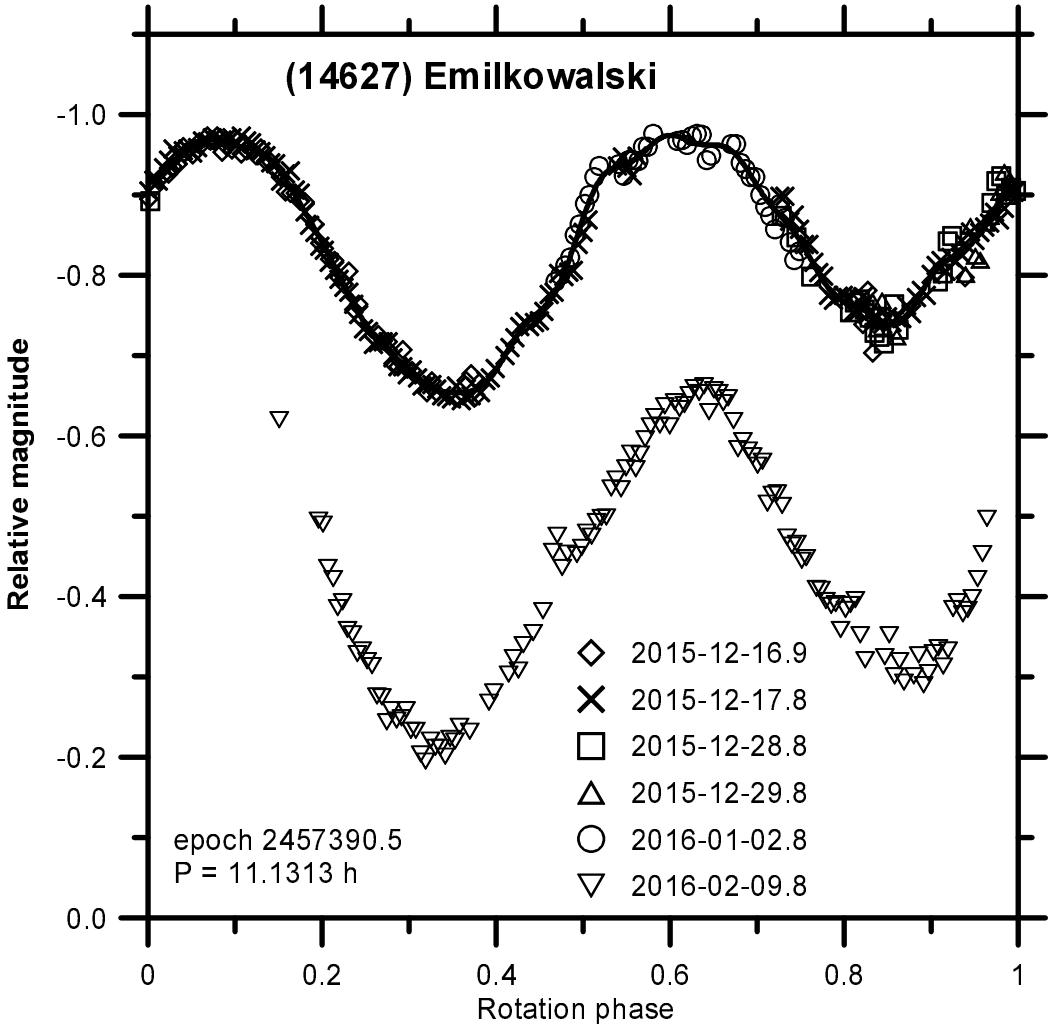


Suppl. Fig. 18. Rotational lightcurves of (14627) Emilkowalski in 2015–2016.

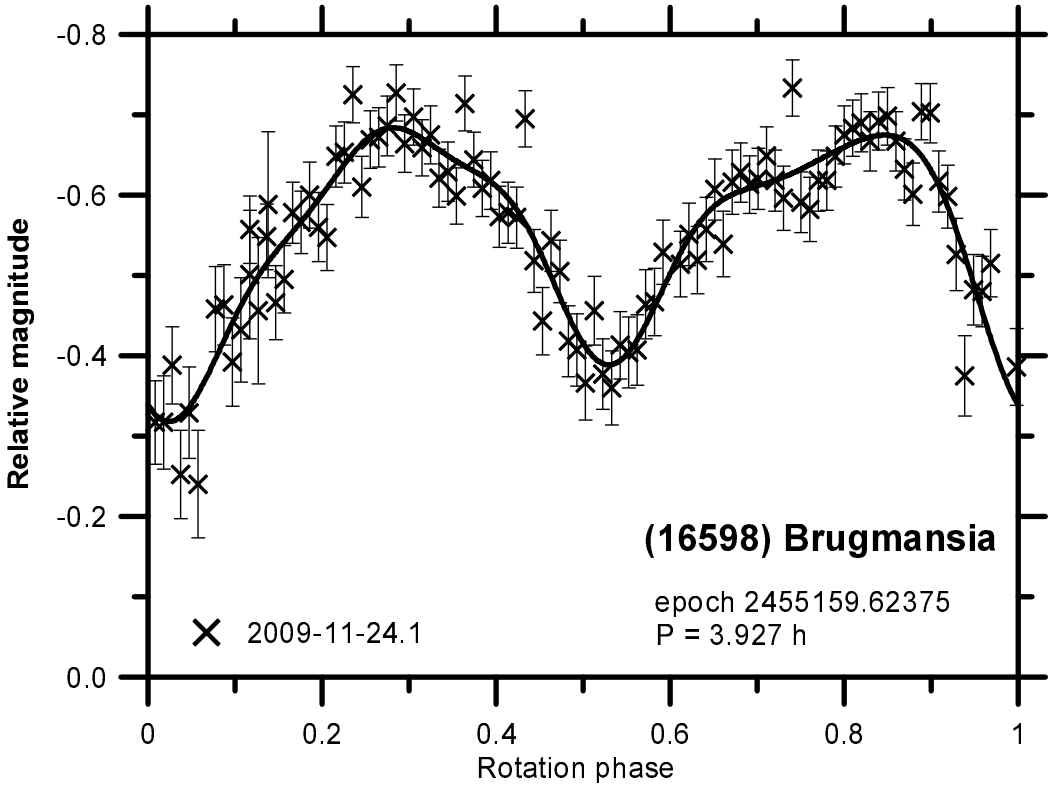


Suppl. Fig. 19. Rotational lightcurve of (16598) Brugmansia in November 2009.

### (16598) Brugmansia

We observed this asteroid from Simeiz on 2009-11-24 and from Ondřejov, Abastumani, SRO and Sugarloaf Mountain on 7 nights during 2013-10-10 to 30. The Ondřejov observations were absolutely calibrated in the Cousins R system using Landolt (1992) standards to an accuracy level of 0.015 mag; the observations from the other stations were on relative (differential) magnitude scales. We derived a period of $3.9272 \pm 0.0003$ h with a lightcurve amplitude of 0.30 mag in October 2013, while it was 0.37 mag on 2009-11-24. The asteroid's mean absolute R magnitude is $H_R = 14.24 \pm 0.24$, assuming the slope parameter $G = 0.15 \pm 0.20$. Our lightcurve data are shown in Suppl. Figs. 19 to 20.

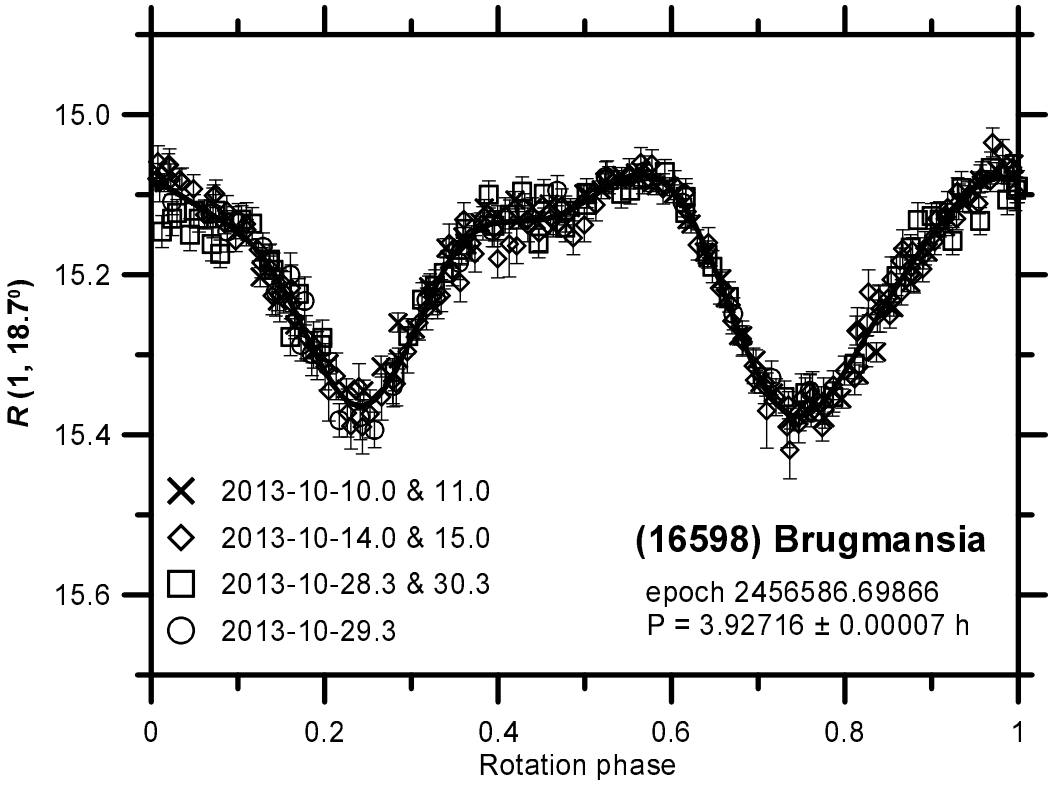


Suppl. Fig. 20. Rotational lightcurve of (16598) Brugmansia in October 2013.

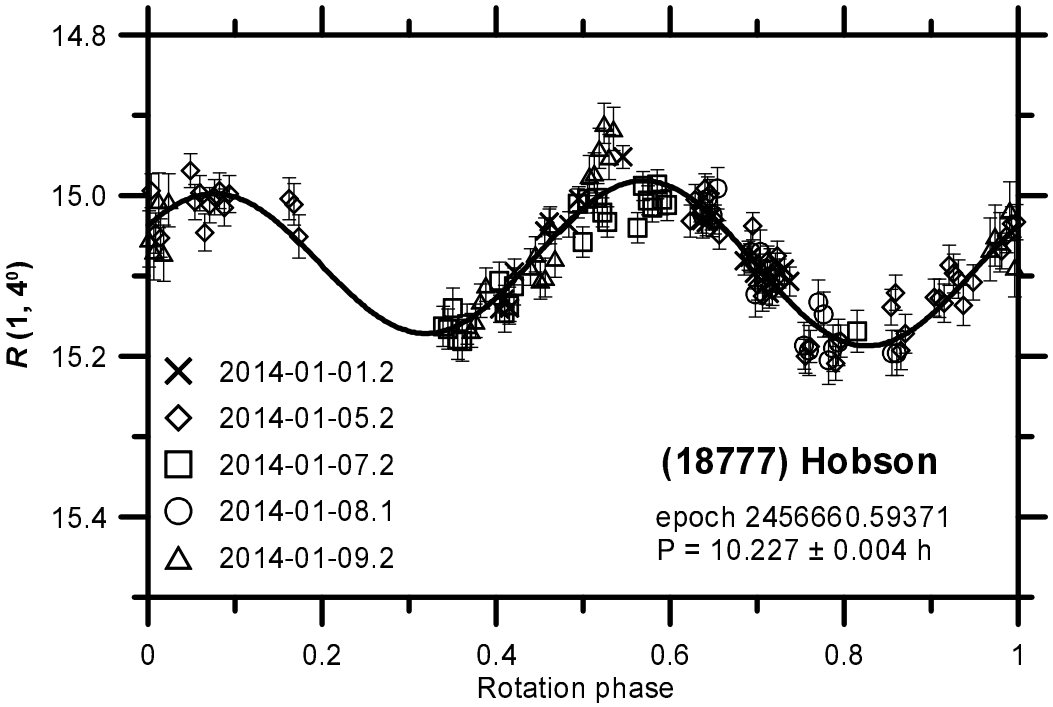


Suppl. Fig. 21. Rotational lightcurve of (18777) Hobson.

### (18777) Hobson

We observed this asteroid from La Silla on 5 nights during 2014-01-01.2 to 09.2. The observations were absolutely calibrated in the Johnson-Cousins VR system using Landolt (1992) standards to an accuracy level of 0.01–0.015 mag. We derived a period of $10.227 \pm 0.004$ h with a lightcurve amplitude of 0.21 mag. For the period derivation, we assumed it is a lightcurve with two pairs maxima/minima per period. There is a small but not zero probability that it has actually four maxima/minima per period (see Harris et al. 2014) and in such case the rotation period is twice the derived period above. On 2014-01-01 we measured the color index $(V - R) = 0.477 \pm 0.01$. We derived the asteroid's mean absolute R magnitude $H_R = 14.68 \pm 0.04$ and the slope parameter $G = 0.08 \pm 0.10$. Our lightcurve data are shown in Suppl. Fig. 21.

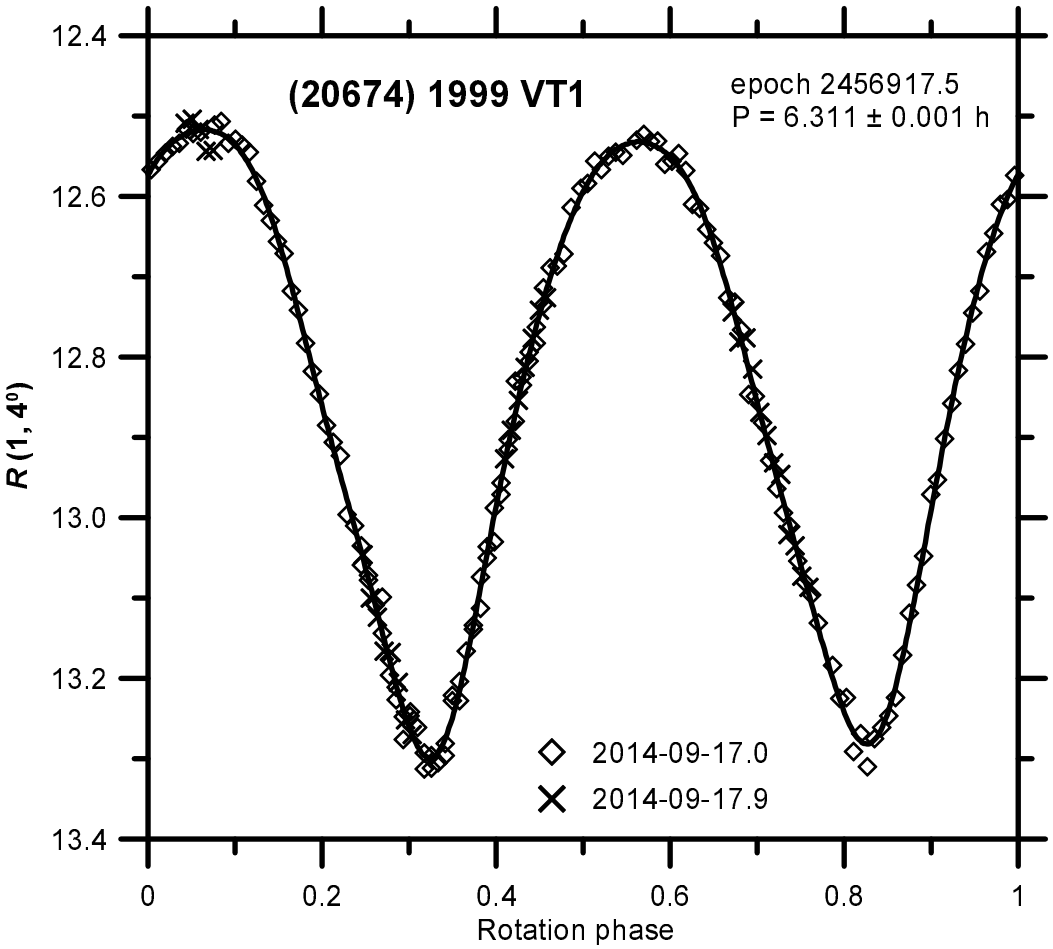


Suppl. Fig. 22. Rotational lightcurve of (20674) 1999 VT1.

### (20674) 1999 VT1

We observed this asteroid from Ondřejov on 2 nights 2014-09-17.0 and 17.9. The observations were absolutely calibrated in the Cousins R system using Landolt (1992) standards to an accuracy level of 0.01 mag. We derived a period of 6.311±0.001 h with a lightcurve amplitude of 0.78 mag. The asteroid's mean absolute R magnitude is $H_R = 12.43 \pm 0.03$, assuming the slope parameter $G = 0.12 \pm 0.08$. Our lightcurve data are shown in Suppl. Fig. 22.

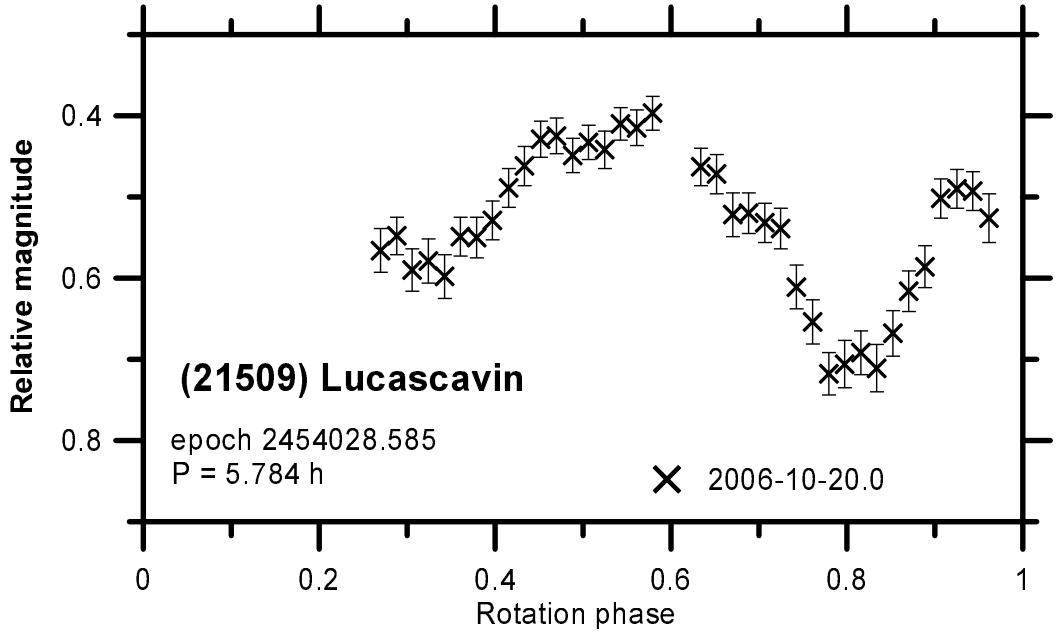


Suppl. Fig. 23. Rotational lightcurve of (21509) Lucascavin in 2006.

### (21509) Lucascavin

We observed this asteroid from Simeiz on 2006-10-20, from Ondřejov and Simeiz on 3 nights 2013-10-30, 31 and 11-01 and from La Silla on 3 nights 2016-09-04, 08 and 10. The La Silla and Ondřejov observations were absolutely calibrated in the Johnson-Cousins VR system using Landolt (1992) standards to an accuracy level of 0.01 mag; the Simeiz runs were taken on relative (differential) magnitude scales. We derived periods of $5.784 \pm 0.004$ h and $5.7891 \pm 0.0008$ h with lightcurve amplitudes of 0.23 and 0.25 mag in 2013 and 2016, respectively. The amplitude was $\geq 0.30$ mag on 2006-10-20. On 2016-09-04.0 we measured the color index $(V - R) = 0.474 \pm 0.016$. The mean absolute R magnitude was $H_R = 14.67 \pm 0.07$ and $14.68 \pm 0.07$ in 2013 and 2016, respectively, both derived assuming $G = 0.24 \pm 0.11$. Our lightcurve data are shown in Suppl. Figs. 23 to 25.

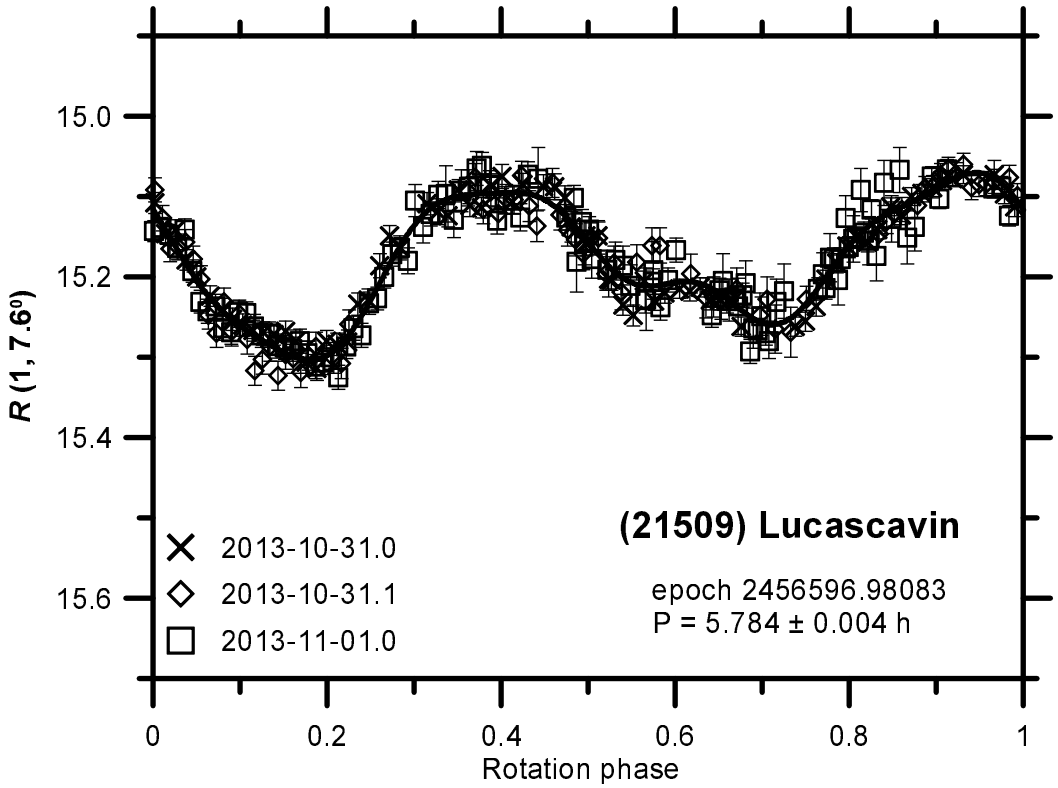


Suppl. Fig. 24. Rotational lightcurve of (21509) Lucascavin in 2013.

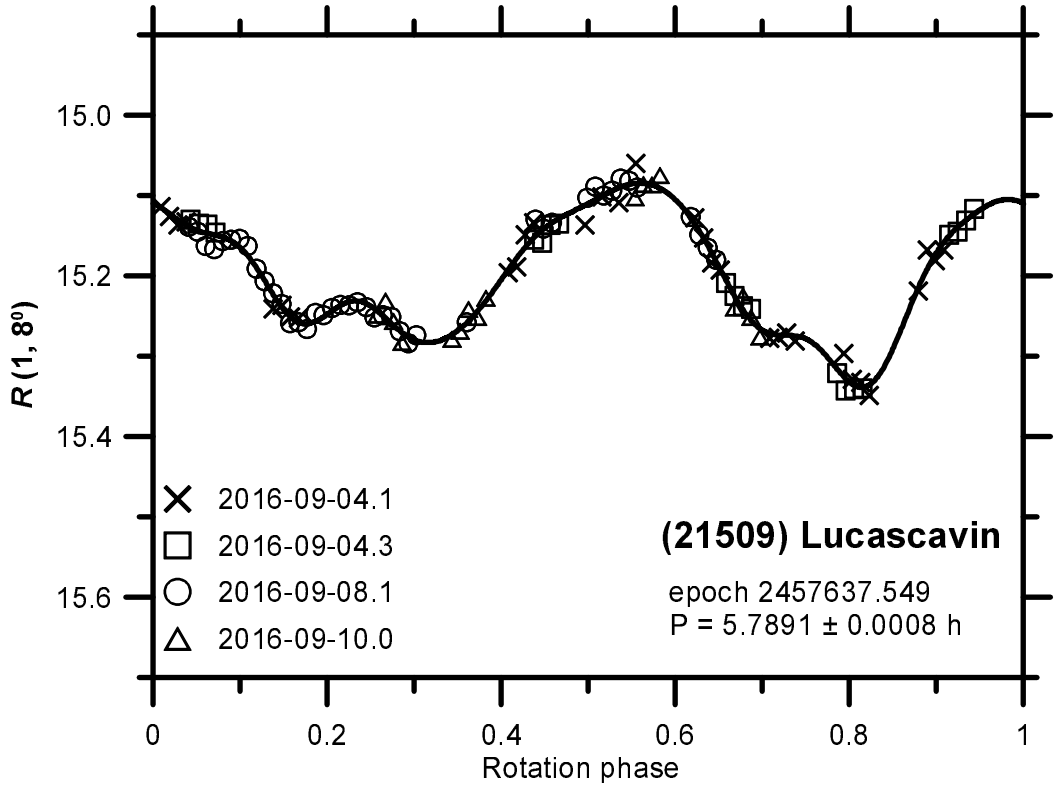


Suppl. Fig. 25. Rotational lightcurve of (21509) Lucascavin in 2016.

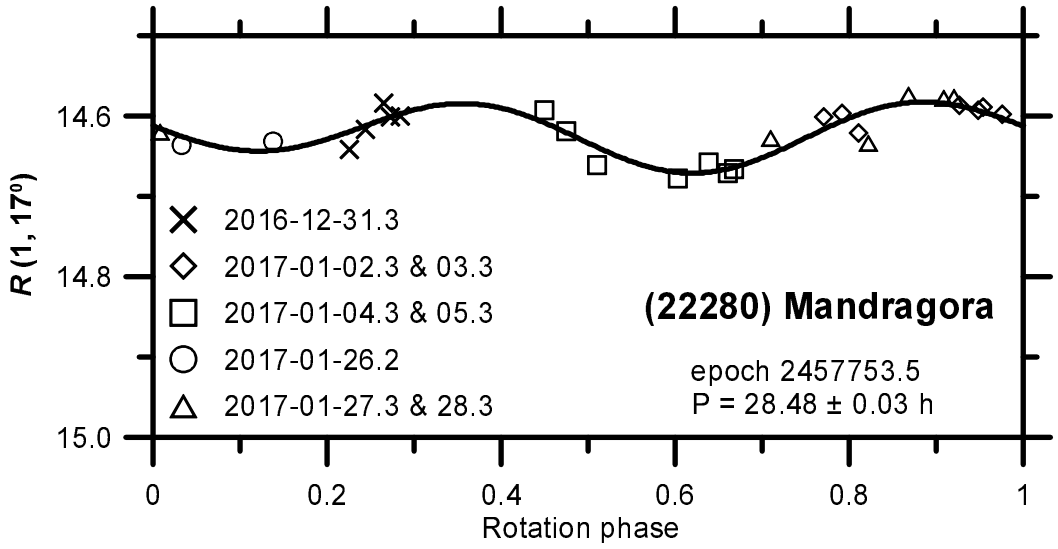


Suppl. Fig. 26. Rotational lightcurve of (22280) Mandragora.

### (22280) Mandragora

We observed this asteroid from La Silla on 8 nights during 2016-12-31 to 2017-01-28. The observations were absolutely calibrated in the Johnson-Cousins VR system using Landolt (1992) standards to an accuracy level of 0.01 mag. We derived a likely period of $28.48 \pm 0.03$ h with a lightcurve amplitude of 0.09 mag. For the low amplitude, this is an $U = 2$ result; we cannot rule out other periods with different numbers of maxima/minima per rotation. On 2016-12-31.4 we measured the color index $(V-R) = 0.405 \pm 0.012$. We derived the asteroid's mean absolute R magnitude $H_R = 13.62 \pm 0.07$ and the slope parameter $G = 0.07 \pm 0.05$. Our lightcurve data are shown in Suppl. Fig. 26.

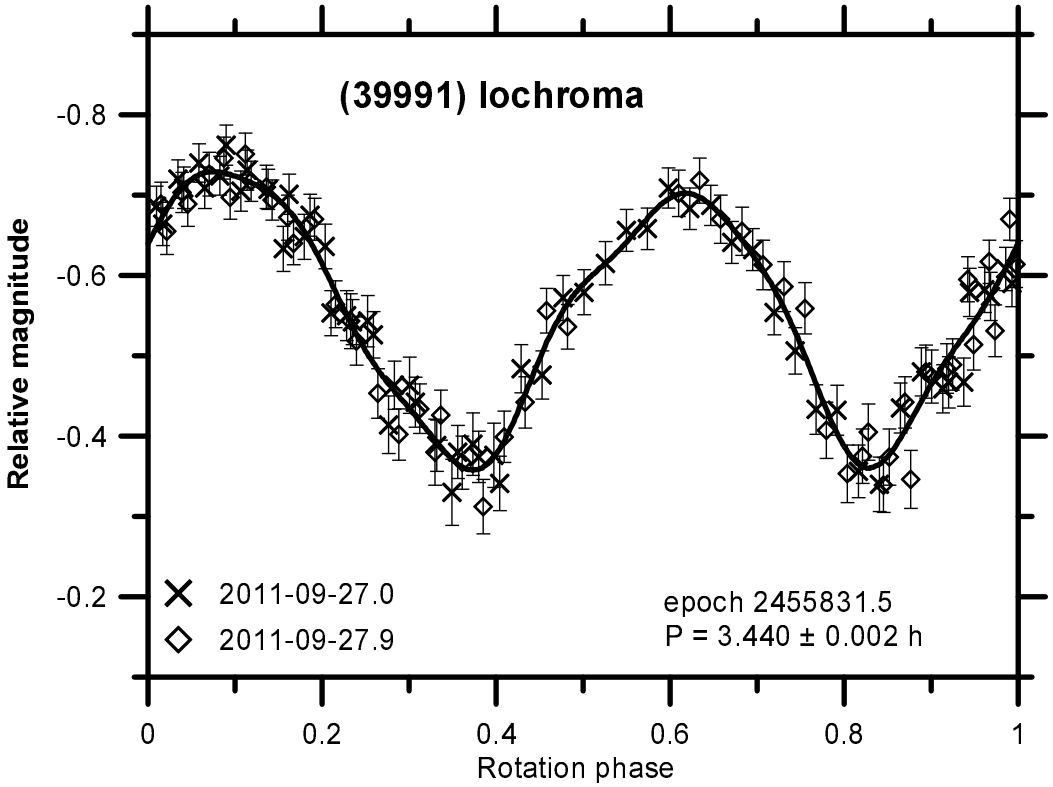


Suppl. Fig. 27. Rotational lightcurve of (39991) Iochroma in 2011.

### (39991) Iochroma

We observed this asteroid from Skalnaté Pleso on 2 nights 2011-09-27.0 and 27.9 and on La Silla on 2017-01-26.3. While the La Silla observations were absolutely calibrated in the Johnson-Cousins VR system using Landolt (1992) standards to an accuracy level of 0.01 mag, the Skalnaté Pleso observations were on relative (differential) magnitude scales. We derived a period of 3.440± 0.002 h with a lightcurve amplitude of 0.37 mag from the 2011 data. On 2017-01-26 we measured the color index $(V - R) = 0.510 \pm 0.012$. We derived the asteroid's mean absolute R magnitude $H_R = 14.28 \pm 0.14$, assuming the slope parameter $G = 0.24 \pm 0.11$. Our lightcurve data are shown in Suppl. Figs. 27 and 28.

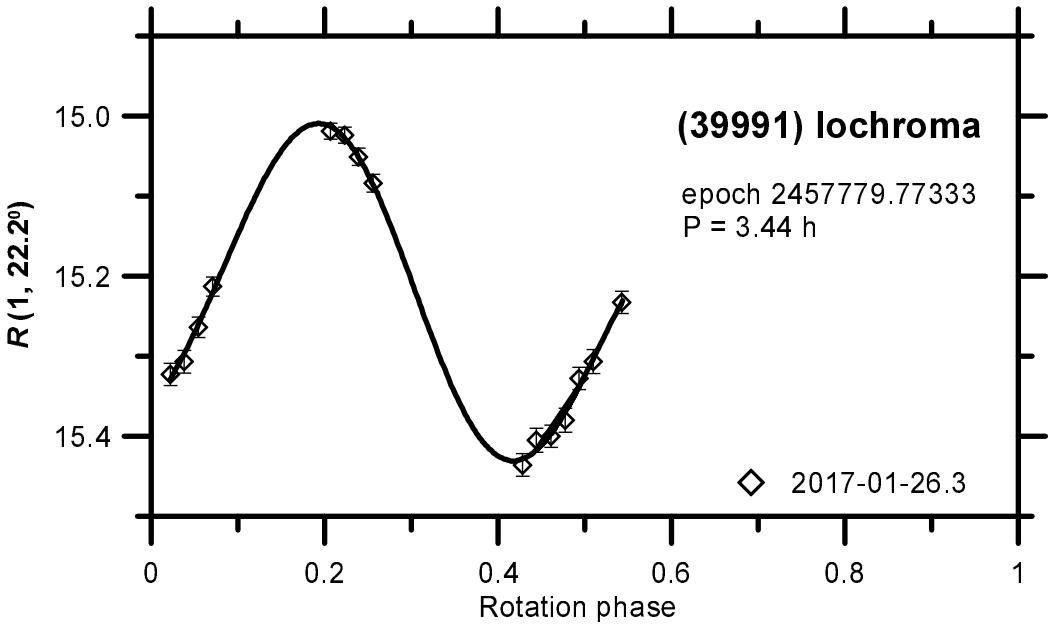


Suppl. Fig. 28. Rotational lightcurve of (39991) Iochroma in 2017.

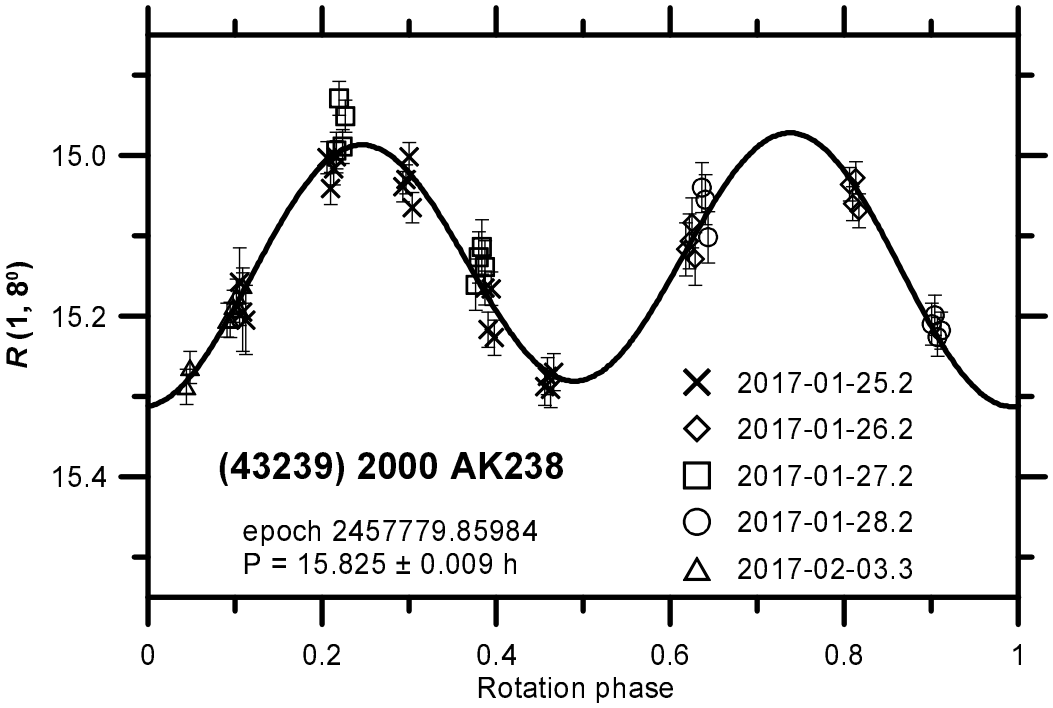


Suppl. Fig. 29. Rotational lightcurve of (43239) 2000 AK238.

### (43239) 2000 AK238

We observed this asteroid from La Silla on 5 nights during 2017-01-25 to 02-03. The observations were absolutely calibrated in the Johnson-Cousins VR system using Landolt (1992) standards to an accuracy level of 0.01–0.015 mag. We derived a period of 15.825±0.009 h (U = 3-) with a lightcurve amplitude of 0.34 mag. On 2017-02-03 we measured the color index $(V-R) = 0.396 \pm 0.017$. We derived the asteroid's mean absolute R magnitude $H_R = 14.50 \pm 0.04$, assuming the cluster primary's slope parameter $G = 0.07 \pm 0.05$ (see the section on 22280 above). Our lightcurve data are shown in Suppl. Fig. 29.

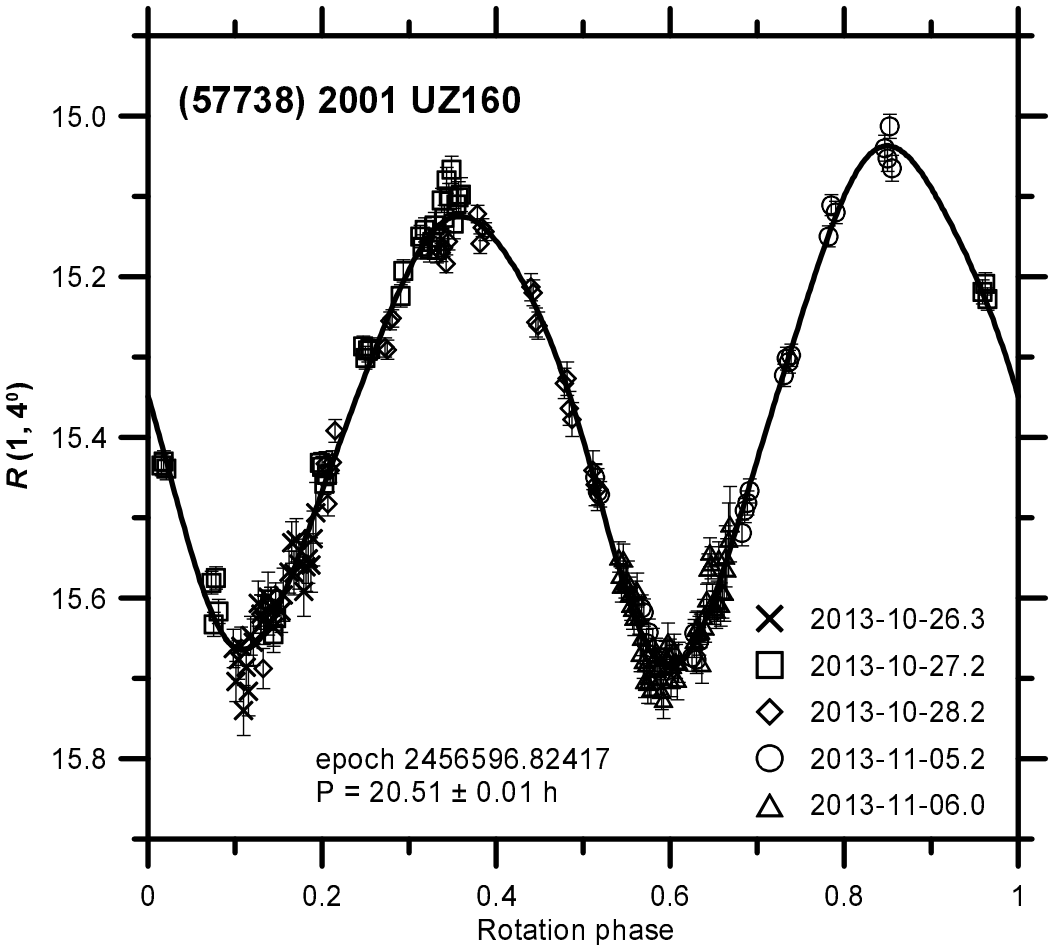


Suppl. Fig. 30. Rotational lightcurve of (57738) 2001 UZ160.

### (57738) 2001 UZ160

We observed this asteroid from La Silla on 4 nights during 2013-10-26.3 to 11-05.2 and from Nauchny on night 2013-11-06.0. The La Silla observations were absolutely calibrated in the Johnson-Cousins VR system using Landolt (1992) standards to an accuracy level of 0.01 mag, while the observations from Nauchny were taken on a relative (differential) magnitude scale. We derived a period of $20.51 \pm 0.01$ h with a lightcurve amplitude of 0.65 mag. On 2013-10-26 we measured the color index $(V - R) = 0.46 \pm 0.02$. We derived the asteroid's mean absolute R magnitude $H_R = 14.95 \pm 0.04$, assuming the slope parameter $G = 0.08 \pm 0.10$. Our lightcurve data are shown in Suppl. Fig. 30.

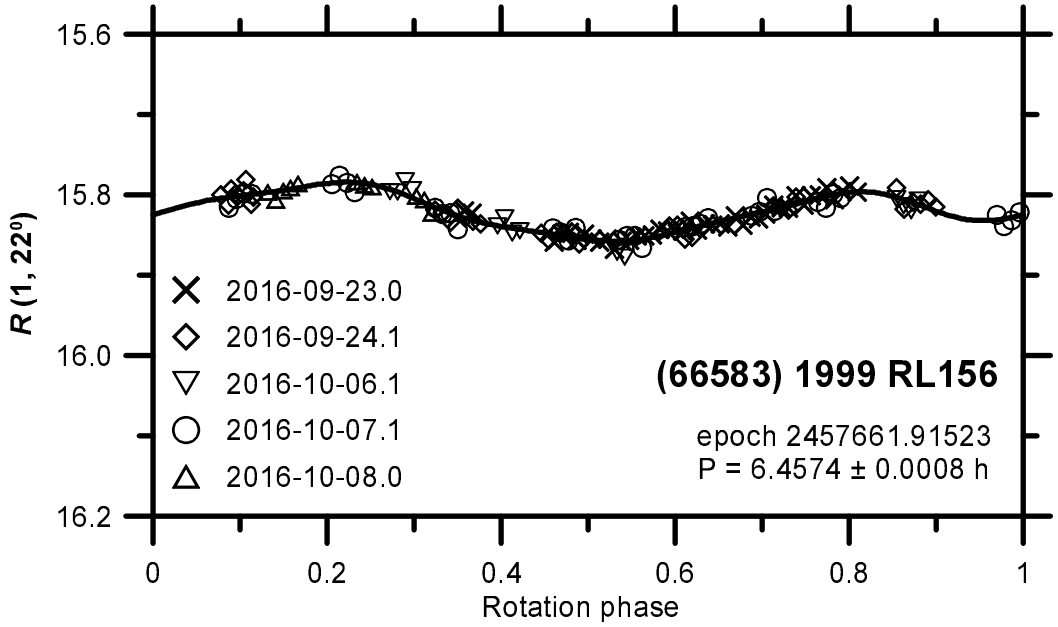


Suppl. Fig. 31. Rotational lightcurve of (66583) 1999 RL156.

### (66583) 1999 RL156

We observed this asteroid from La Silla on 5 nights during 2016-09-23 to 10-08. The observations were absolutely calibrated in the Johnson-Cousins VR system using Landolt (1992) standards to an accuracy level of 0.01 mag. We derived a period of $6.457 \pm 0.001$ h with a lightcurve amplitude of 0.07 mag. For the low amplitude, this is an $U = 2$ result; we cannot rule out a period twice as long with twice as many maxima/minima per rotation. On 2016-09-23.1 we measured the color index $(V - R) = 0.355 \pm 0.01$. We derived the asteroid's mean absolute R magnitude $H_R = 14.55 \pm 0.14$ and the slope parameter $G = 0.01 \pm 0.08$. Our lightcurve data are shown in Suppl. Fig. 31.

### (81337) 2000 GP36

We observed this asteroid from Maidanak on 3 nights 2014-08-24, 25 and 09-01 and from Rozhen on 2 nights 2015-11-13 and 14. The observations from Rozhen were absolutely calibrated in the Cousins R system to an accuracy level of 0.03–0.04 mag, while the Maidanak observations were on relative (differential) magnitude scales. From the 2014 observations we derived a period of $10.028 \pm 0.001$ h with a lightcurve amplitude of 1.22 mag, assuming zero amplitudes of the odd lightcurve harmonics (that is equivalent to a lightcurve symmetry with $P/2$; a plausible assumption for the high-amplitude lightcurve). From the 2015 observations we derived a period of $10.027 \pm 0.006$ h with a lightcurve amplitude of 1.36 mag. The mean absolute R magnitude $H_R = 14.90 \pm 0.04$ was derived, assuming the Schulhof's $G = 0.24 \pm 0.02$ (Vokrouhlický et al. 2016a), and it converts to $H = 15.39 \pm 0.06$, assuming $(V - R) = 0.49 \pm 0.05$ (see Vokrouhlický et al. 2016a). Our lightcurve data are shown in Suppl. Figs. 32 to 33.

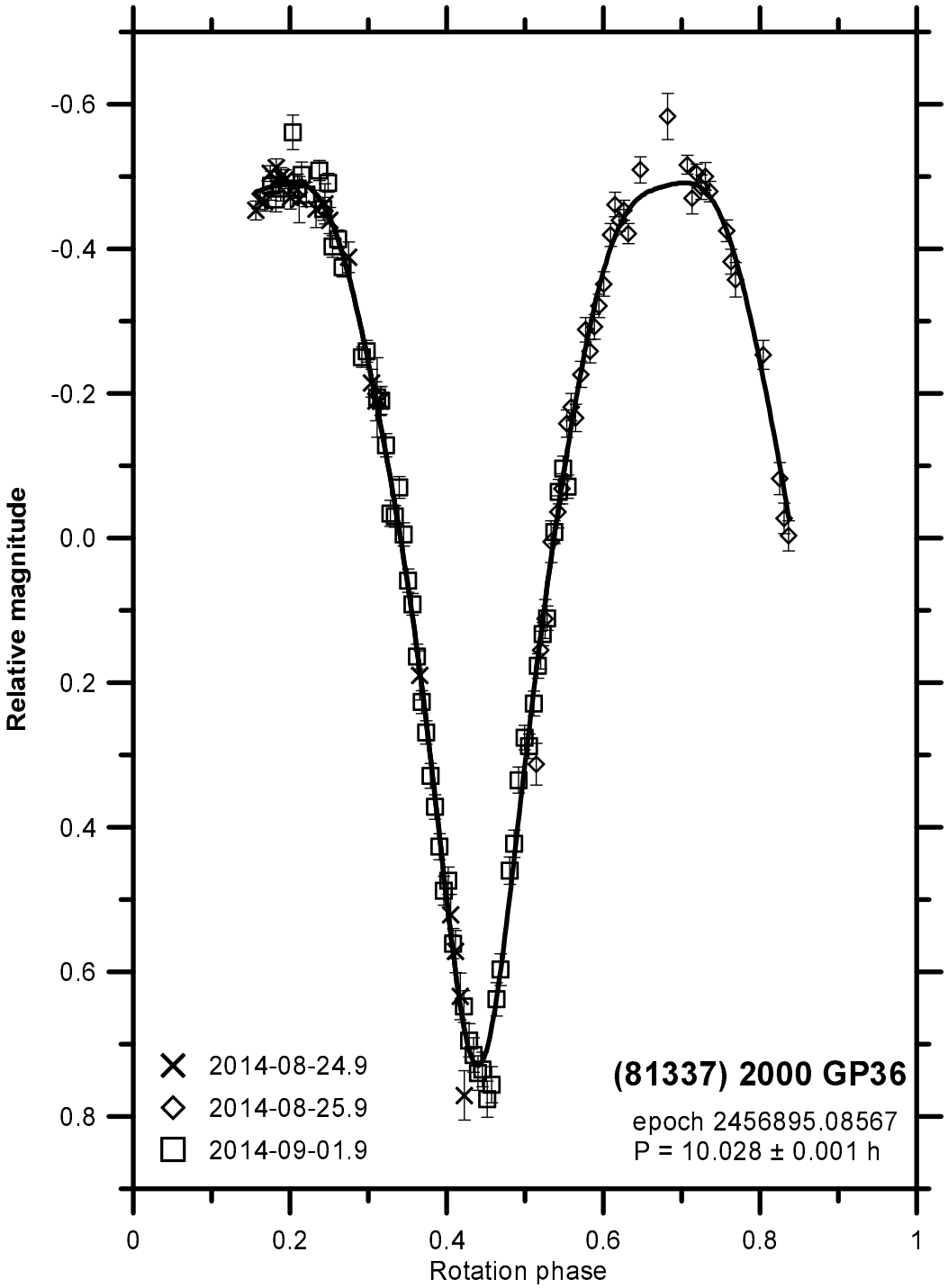


Suppl. Fig. 32. Rotational lightcurve of (81337) 2000 GP36 in 2014.

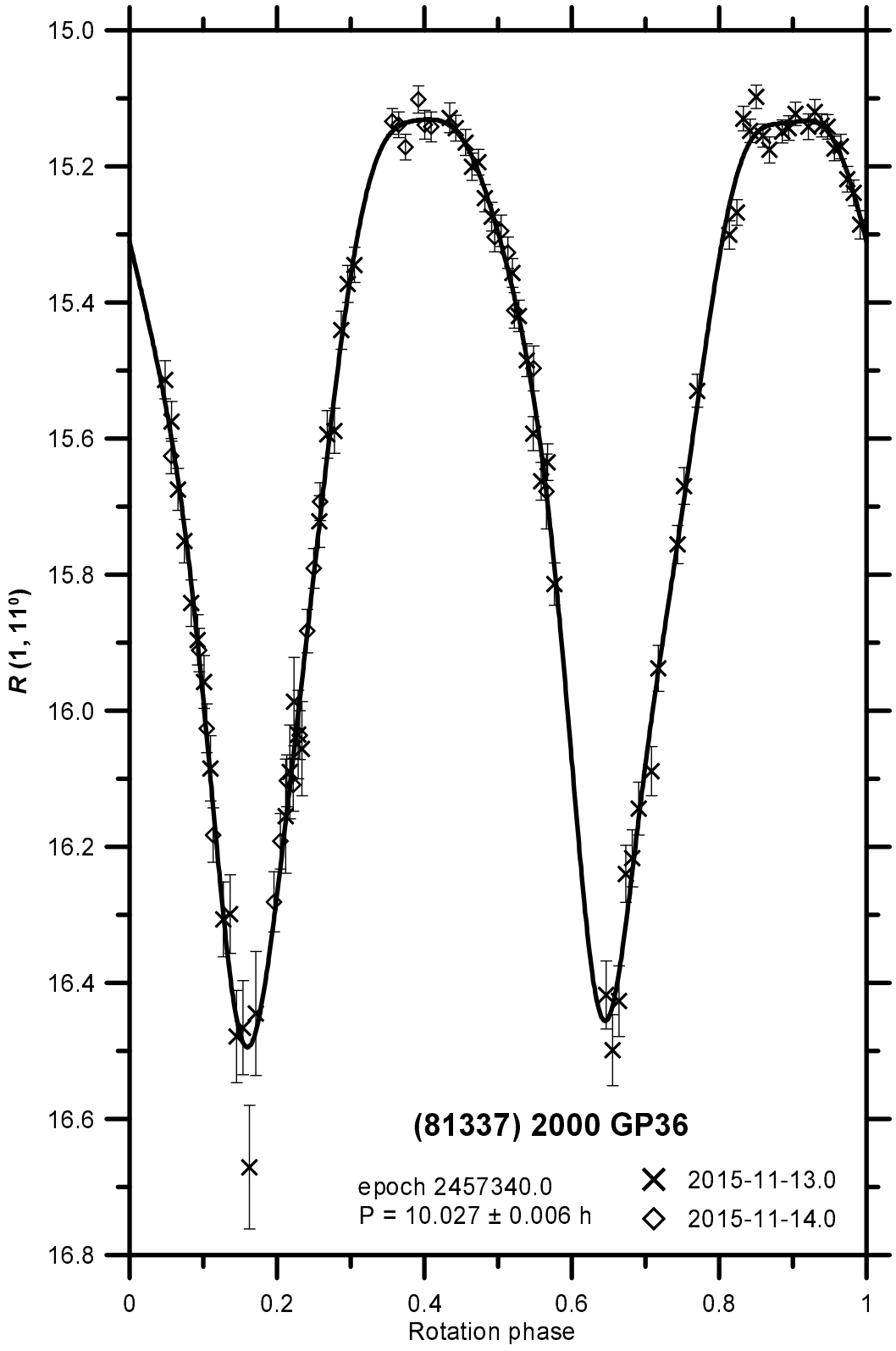


Suppl. Fig. 33. Rotational lightcurve of (81337) 2000 GP36 in 2015.

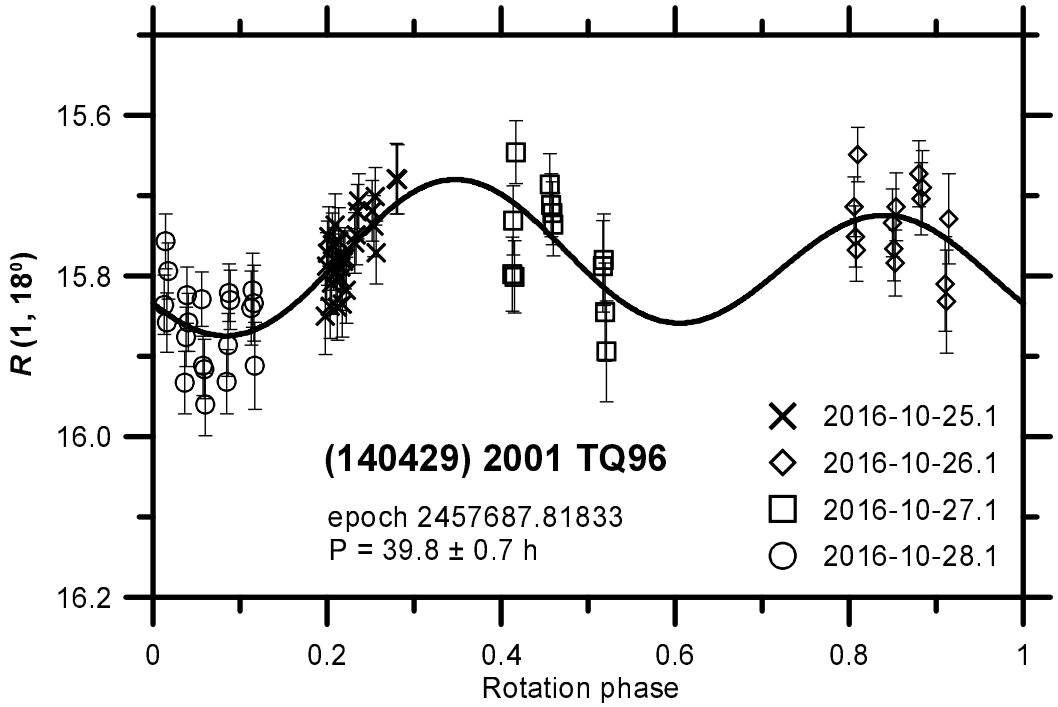


Suppl. Fig. 34. Rotational lightcurve of (140429) 2001 TQ96.

### (140429) 2001 TQ96

We observed this asteroid from La Silla on 4 nights 2016 October 25 to 28. The observations were absolutely calibrated in the Cousins R system using Landolt (1992) standards to an accuracy level of 0.01 mag. We derived a probable period of $39.8 \pm 0.7$ h, assuming two pairs of maxima/minima per period, with a lightcurve amplitude of 0.19 mag. We derived the asteroid's mean absolute R magnitude $H_R = 14.81 \pm 0.10$, assuming the slope parameter $G = 0.12 \pm 0.08$. Our lightcurve data are shown in Suppl. Fig. 34.

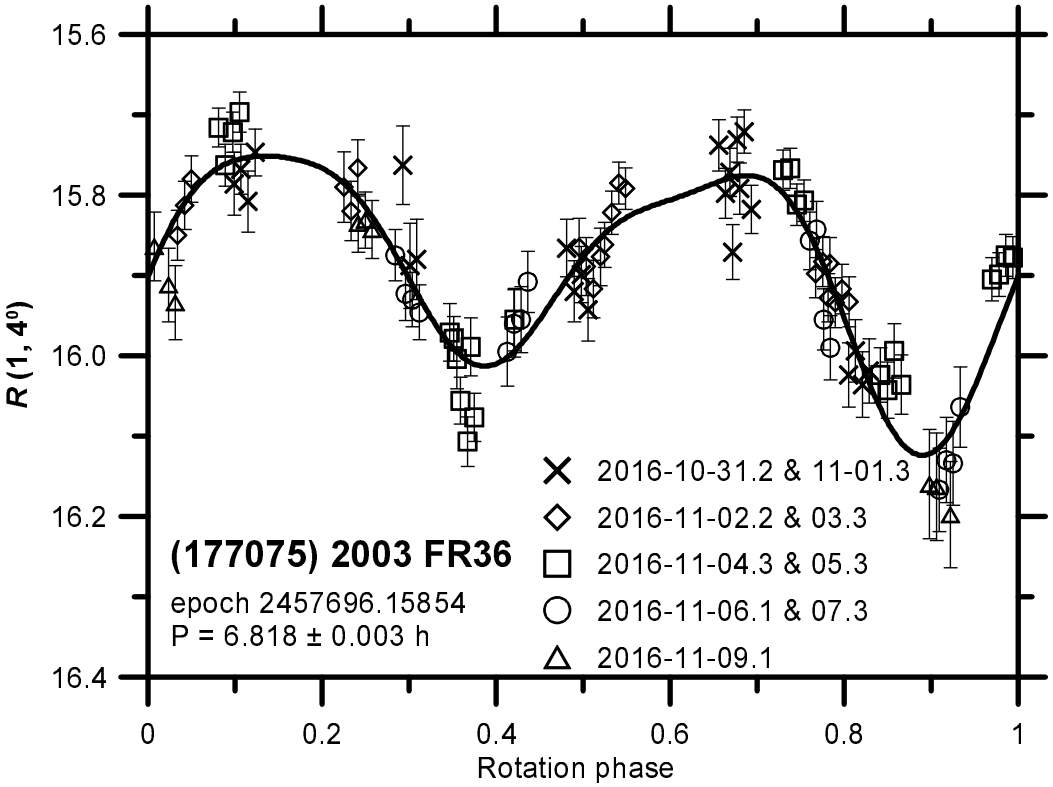


Suppl. Fig. 35. Rotational lightcurve of (177075) 2003 FR36.

### (177075) 2003 FR36

We observed this asteroid from La Silla on 9 nights during 2016 October 31 to November 9. The observations were absolutely calibrated in the Cousins R system using Landolt (1992) standards to an accuracy level of 0.01–0.015 mag. We derived a period of 6.818±0.003 h with a lightcurve amplitude of 0.37 mag. We derived the asteroid's mean absolute R magnitude $H_R = 15.50 \pm 0.03$, assuming the slope parameter $G = 0.12 \pm 0.08$. Our lightcurve data are shown in Suppl. Fig. 35.

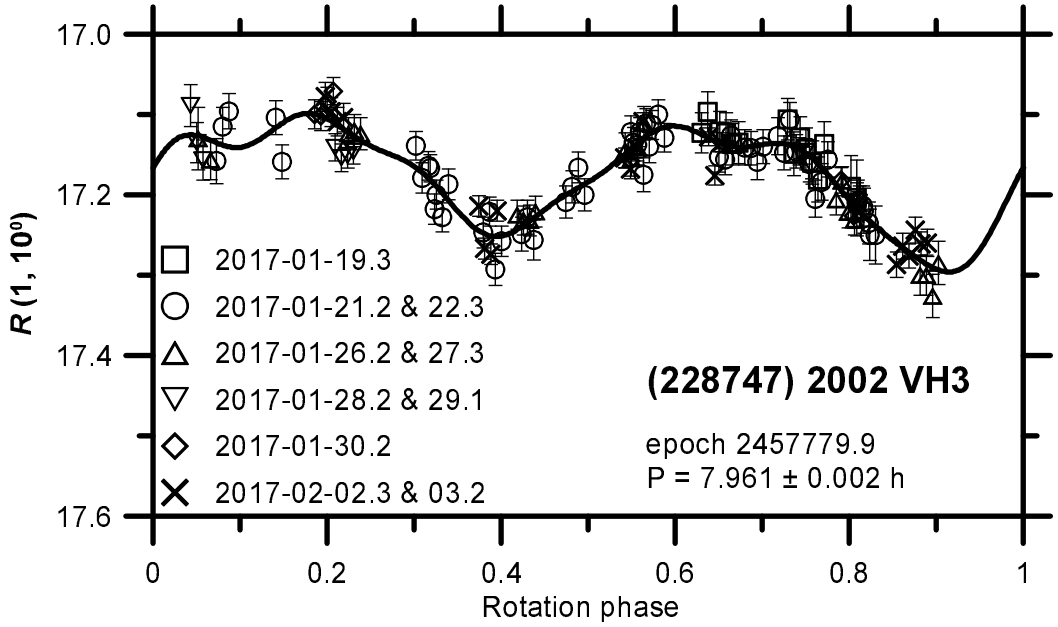


Suppl. Fig. 36. Rotational lightcurve of (228747) 2002 VH3.

### (228747) 2002 VH3

We observed this asteroid from La Silla on 10 nights during 2017 January 19 to February 3. The observations were absolutely calibrated in the Johnson-Cousins VR system using Landolt (1992) standards to an accuracy level of 0.01–0.02 mag. We derived a period of 7.961 ± 0.002 h (U = 3-) with a lightcurve amplitude of 0.20 mag. On 2017-02-02.3 we measured the color index $(V - R) = 0.497 \pm 0.019$. We derived the asteroid's mean absolute R magnitude $H_R = 16.66 \pm 0.04$ and the slope parameter $G = 0.34 \pm 0.06$. Our lightcurve data are shown in Suppl. Fig. 36.

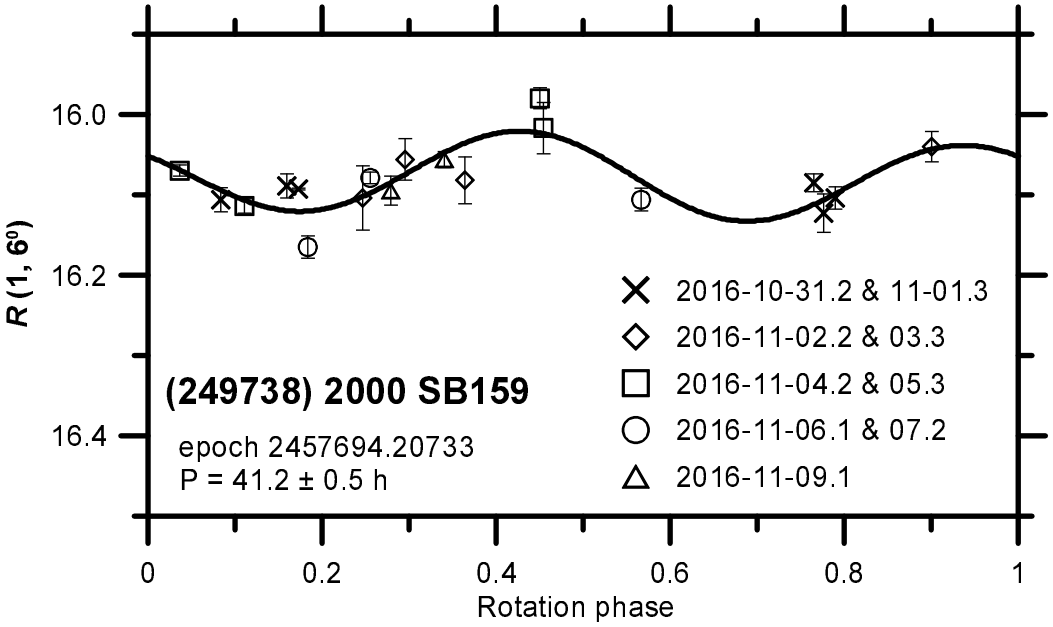


Suppl. Fig. 37. Rotational lightcurve of (249738) 2000 SB159.

### (249738) 2000 SB159

We observed this asteroid from La Silla on 9 nights during 2016 October 31 to November 9. The observations were absolutely calibrated in the Cousins R system using Landolt (1992) standards to an accuracy level of 0.01 mag. We derived a period of $41.2 \pm 0.5$ h, assuming rotational lightcurve predominated by the 2nd harmonic. The lightcurve amplitude was 0.11 mag. We derived the asteroid's mean absolute R magnitude $H_R = 15.58 \pm 0.04$, assuming the slope parameter $G = 0.12 \pm 0.08$. Our lightcurve data are shown in Suppl. Fig. 37.

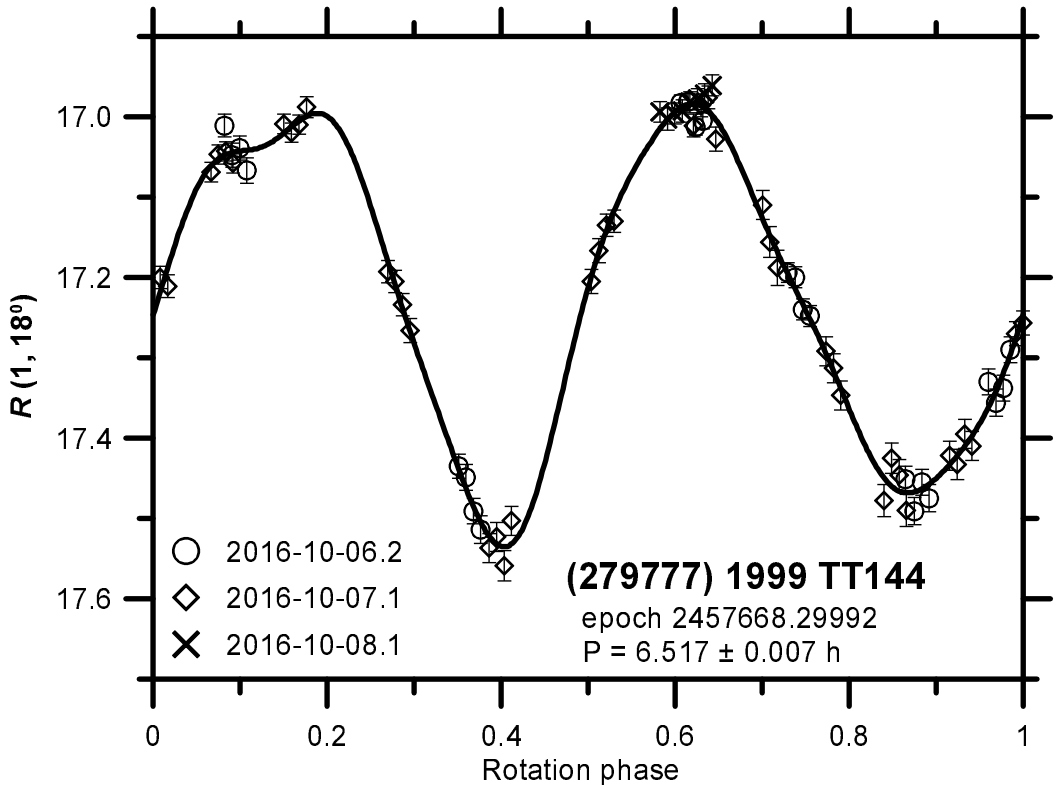


Suppl. Fig. 38. Rotational lightcurve of (279777) 1999 TT144.

### (279777) 1999 TT144

We observed this asteroid from La Silla on 3 nights 2016-10-06 to 08. The observations were absolutely calibrated in the Johnson-Cousins VR system using Landolt (1992) standards to an accuracy level of 0.01 mag. We derived a period of $6.517 \pm 0.007$ h with a lightcurve amplitude of 0.55 mag. On 2016-10-08.1 we measured the color index $(V - R) = 0.359 \pm 0.017$. We derived the asteroid's mean absolute R magnitude $H_R = 16.10 \pm 0.11$, assuming the primary's slope parameter $G = 0.01 \pm 0.08$. Our lightcurve data are shown in Suppl. Fig. 38.

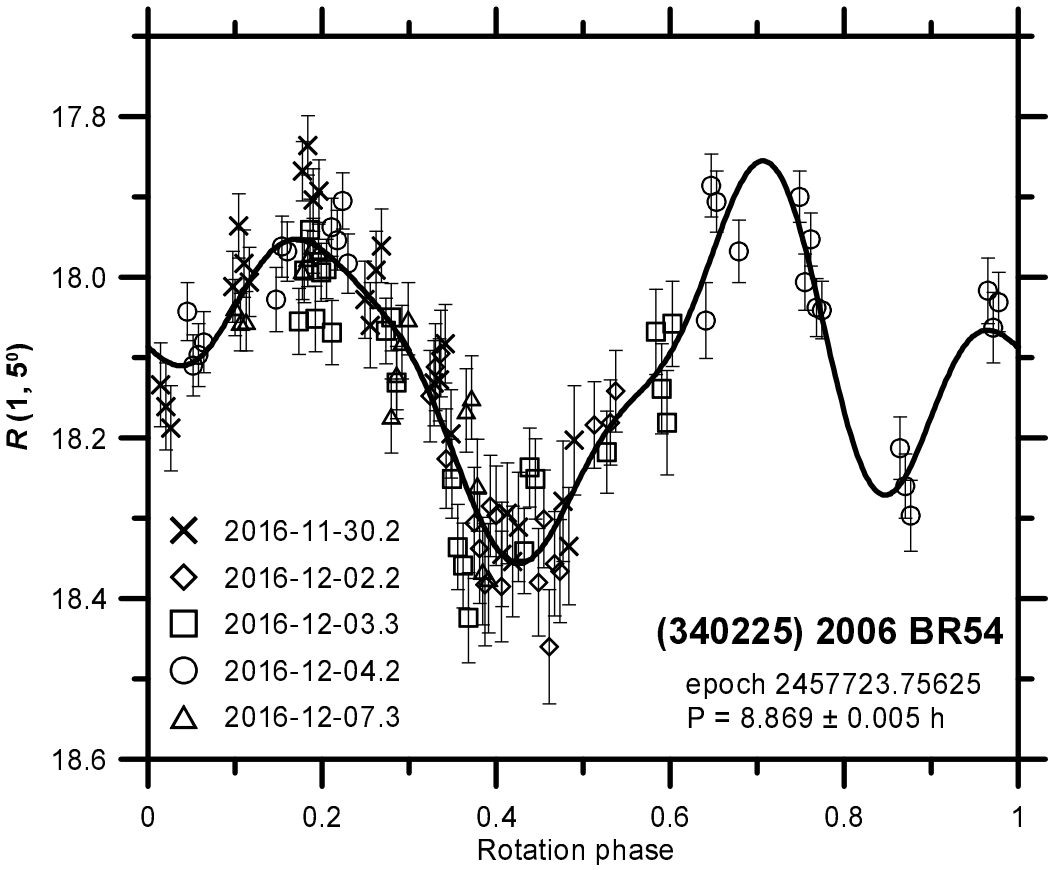


Suppl. Fig. 39. Rotational lightcurve of (340225) 2006 BR54.

### (340225) 2006 BR54

We observed this asteroid from La Silla on 5 nights 2016-11-30 to 12-07. The observations were absolutely calibrated in the Cousins R system using Landolt (1992) standards to an accuracy level of 0.01–0.015 mag. We derived a period of $8.869 \pm 0.005$ h with a lightcurve amplitude of 0.50 mag. We derived the asteroid's mean absolute R magnitude $H_R = 17.71 \pm 0.05$, assuming $G = 0.24 \pm 0.11$. Our lightcurve data are shown in Suppl. Fig. 39.

**References**

Carruba, V., Nesvorný, D., Vokrouhlický, D., 2016. Detection of the YORP effect for small asteroids in the Karin cluster. Astron. J. 151:164 (11pp).

Carruba, V., Vokrouhlický, D., Nesvorný, D., 2017. Detection of the Yarkovsky effect for C-type asteroids in the Veritas family. Mon. Not. Roy. Astron. Soc., in press.

Erikson, A., Mottola, S., Lagerros, J.S.V., et al., 2000. The Near-Earth Objects Follow-up Program III. 32 Lightcurves for 12 Objects from 1992 and 1995. Icarus 147, 487–497.

Galád, A., Pravec, P., Gajdoš, Š., et al., 2007. Seven asteroids studied from Modra observatory in the course of binary asteroid photometric campaign. Earth Moon Planets 101, 17–25.

Husárik, M., Kušnirák, P., 2008. Relative photometry of asteroids (1314), (2257), (3541), (4080), (4155), (12081) and (15415). Contributions of the Astronomical Observatory Skalnaté Pleso 38, 47–60.

Krugly, Yu.N., Belskaya, I. N., Shevchenko, V. G., et al., 2002. The Near-Earth Objects Follow-up Program. IV. CCD Photometry in 1996-1999. Icarus 158, 294–304.

Krugly, Yu.N., 2004. Problems of CCD Photometry of Fast-Moving Asteroids. Sol. Syst. Res. 38(3), 241–248.

Landolt, A.U., 1992. UBVRI photometric standard stars in the magnitude range 11.5-16.0 around the celestial equator. Astron. J. 104, 340–371, 436–491.

Lang, D., Hogg, D.W., Mierle, K., et al., 2010. Astrometry.net: Blind astrometric calibration of arbitrary astronomical images. Astron. J. 137, 1782-1800.

Mottola, S., De Angelis, G., Di Martino, M., et al., 1995. The near-Earth objects follow-up program: first results. Icarus 117, 62–70.

Nesvorný, D., Bottke, W.F., 2004. Detection of the Yarkovsky effect for main-belt asteroids. Icarus 170, 324–342.

Nesvorný, D., Bottke, W.F., Dones, L., Levison, H.F., 2002. The recent breakup of an asteroid in the main-belt region. Nature 417, 720–722.

Nesvorný, D., Bottke, W.F., Levison, H.F., et al., 2003. Recent origin of the Solar System dust bands. Astrophys. J. 591, 486–497.

Nesvorný, D., Vokrouhlický, D., 2006. New candidates for recent asteroid breakups. Astron. J. 132, 1950–1958.

Nesvorný, D., Vokrouhlický, D., Bottke, W.F., 2006. The Breakup of a Main-

Belt Asteroid 450 Thousand Years Ago. Science 312, 1490.

Nesvorný, D., Brož, M., Carruba, V., 2015. Identification and dynamical properties of asteroid families. In: Asteroids IV (eds. P. Michel et al.), University of Arizona Press, Tucson, 297–321.

Novaković, B., 2010. Portrait of Theobalda as a young asteroid family. Mon. Not. Roy. Astron. Soc. 407, 1477–1486.

Novaković, B., Dell'Oro, A., Cellino, A., et al., 2012. Recent collisional jet from a primitive asteroid. Mon. Not. Roy. Astron. Soc. 425, 338–346.

Novaković, B., Hsieh, H.H., Cellino, A., et al., 2014. Discovery of a young asteroid cluster associated with P/2012 F5 (Gibbs). Icarus 231, 300-309.

Pravec, P., Scheirich, P., Kušnirák, P., et al., 2006. Photometric survey of binary near-Earth asteroids. Icarus 181, 63–93.

Pravec, P., Vokrouhlický, D., 2009. Significance analysis of asteroid pairs. Icarus 204, 580–588.

Pravec, P., Vokrouhlický, D., Polishook, D., et al., 2010. Formation of asteroid pairs by rotational fission. Nature 466, 1085–1088.

Pravec, P., Scheirich, P., Ďurech, J., et al. 2014. The tumbling spin state of (99942) Apophis. Icarus 233, 48–60.

Rosaev, A., Plávalová, E., 2017. On the young family of 18777 Hobson. Icarus 282, 326–332.

Skiff, B.A., 2007. BVRI Photometry of Faint Field Stars. VizieR On-line Data Catalog: II/277, Lowell Observatory.

Vokrouhlický, D., Ďurech, J., Michałowski, T., et al., 2009. Datura family: the 2009 update. Astron. Astrophys. 507, 495–504.

Vokrouhlický, D., Ďurech, J., Pravec, P., et al., 2016. The Schulhof family: Solving the age puzzle. Astron. J. 151:56 (12pp).

Waszczak, A., Chang, C.-K., Ofek, E. O., et al., 2015. Asteroid Light Curves from the Palomar Transient Factory Survey: Rotation Periods and Phase Functions from Sparse Photometry. Astron. J. 150:75 (35pp).